REVIEWS OF GEOPHYSICS, VOL. 26, NO. 3, PAGES 551–578, AUGUST 1988

VLF Wave Stimulation Experiments in the Magnetosphere from Siple Station, Antarctica

R. A. HELLIWELL

Space, Telecommunications, and Radioscience Laboratory, Stanford University, Stanford, California

The Earth's magnetosphere is host to remarkable very low frequency (VLF) electromagnetic signals of natural origin. One of these, called a whistler, originates in lightning. Others, such as hiss and chorus, originate within the plasma itself. They are important for at least three reasons. First, they reveal the properties of the plasma through which they travel and thus can be used as remote sensing tools. Second, their high intensity and narrow bandwidths indicate the presence of a previously unknown kind of wave particle interaction that converts the kinetic energy of charged particles to coherent electromagnetic radiation. This process is called the coherent wave instability (CWI). Third, energetic charged particles are precipitated into the ionosphere through resonant scattering by these same waves, causing enhanced thermal ionization, X rays, light, and heat. To better understand and use the CWI, controlled VLF signals have been injected into the magnetosphere from Siple Station, Antarctica and received on satellites and near the conjugate point in Quebec, Canada. In addition to reproducing many puzzling natural phenomena, these experiments have provided critical new data on the CWI, laying a foundation for various theories and computer simulations. Key findings are as follows: 1) Coherent VLF signals often exhibit exponential temporal growth (~ 30 dB) and saturation at levels estimated to be of order 5 pT. 2) Temporal growth requires that the input signal exceed a threshold that varies widely with time. The probable cause of the growth threshold is in situ background noise that reduces the efficiency of phase bunching by a coherent input signal whose intensity is comparable to the noise level within the frequency band of the interaction (~ 100 hz). 3) Narrowband triggered emissions can be entrained by Siple frequency ramps of different slope but of much lower (-20 dB) amplitude. The mechanism of entrainment is not yet understood. 4) For two equal amplitude input waves spaced 20 Hz apart, the temporal growth of each component is almost totally suppressed. For larger spacings, 40–100 Hz, the lower frequency is more suppressed than the upper. For $10 < \Delta f < 100$ Hz, unsymmetrical sidebands at integer multiples (up to seventh order) of Δf are created, along with subharmonics. The integer sidebands are attributed to emission growth triggered by one beat and suppressed by the next. Taken together, the spectrum of the stimulated sidebands and sub-harmonics is thus more noise-like than the transmitted spectrum. 5) Simulated hiss shows coalescence of selected noise wavelets into longer and stronger chorus-like emissions, suggesting that chorus and hiss originate in the same mechanism. Future objectives of a VLF wave injection facility include (1) new experiments on the physics of wave growth and wave-induced particle scattering and precipitation, (2) testing of the predictions of theories of VLF wave-particle interaction, (3) development of new techniques for remote sensing and control of space plasmas using VLF techniques, and (4) improvements in the design and operation of VLF communication and navigation systems.

1. INTRODUCTION

1.1. *Nature of Problem*

Remarkable natural electromagnetic signals, or "sounds", are observed in and from the Earth's magnetosphere at very low frequencies (VLF). One type is excited by lightning impulses that are dispersed on magnetic field aligned ducts in the magnetosphere giving rise to an audio frequency tone, most often of descending frequency, called a "whistler". Whistlers together with related naturally occurring signals, such as chorus and hiss, can be heard on long telephone lines, or with the aid of an audio amplifier connected to an antenna. Whistler mode signals carry "fingerprints" of the Earth's plasma and also its magnetic field and hence find use as diagnostic tools for study of the magnetosphere. Although these natural signals are truly astonishing in the variety of their spectral shapes, their uncontrolled nature severely limits their usefulness for quantitative study, especially in the area of wave-particle interaction mechanisms.

The propagation of VLF waves in a magnetized plasma is markedly affected by the dispersion and anisotropy of the medium. In addition, as a result of Doppler-shifted cyclotron resonance with energetic charged particles a coherent VLF signal can be amplified by as much as 40 dB and trigger narrow-band emissions that are comparable in strength to the amplified triggering signal itself. In this mechanism the resonant electrons (energies of the order of 1 to 100 keV) give up a small fraction of their energy to the circularly polarized whistler mode waves traveling in the opposite direction. To explain the relatively small (~1%) bandwidth of the stimulated radiation, it has been proposed that the interaction takes place in an extended resonance region (500–1000 km in length) located near the equatorial plane, as sketched in Figure 1*e* [*Helliwell*, 1967; *Helliwell and Inan*, 1982]. The stimulated radiation comes from electrons that are temporarily phase-bunched by the relatively high amplitude wave in the upstream, or output, segment of the interaction region. This region is in effect a giant distributed amplifier with positive feedback from the output to the input. When the gain of the feedback loop exceeds unity, the

Paper number 8R0280.
8755-1209/88/008R-0280$05.00

oscillation becomes self sustaining, and an external signal is no longer required to maintain the output. The underlying problem associated with these effects is to explain quantitatively the mechanisms by which VLF waves interact with the plasma. An important aspect of this effort is to design and carry out experiments that can test the various models, such as that described above, that have been advanced (see *Carlson* [1987] for review of theories) to explain the observations. A related objective is the development of new methods for monitoring and controlling the magnetosphere and ionosphere, based on both the theoretical and the experimental results. Another application is the design and use of communication and navigation systems involving the ionized regions of the Earth's upper atmosphere, especially in the range 1–30 kHz.

Experiments on the growth and triggering of narrow-band VLF radiation in the magnetosphere were developed as a result of a serendipitous finding that the Morse code dashes from VLF transmitters often trigger VLF emissions [*Helliwell*, 1965]. To exploit this finding, a special VLF transmitter was designed and operated at Siple Station, Antarctica, from 1973 to 1977. The results have provided essential new information on the behavior of coherent VLF radio waves that interact with both the thermal and the energetic electrons in the Earth's plasma envelope. Accounts of this early work are given elsewhere [*Helliwell and Katsufrakis*, 1978]. Later work using an advanced VLF wave injection facility at Siple Station is the subject of the present paper. A sketch of the elements of these experiments is shown in Figure 1*e*.

1.2. *Reasons for Interest*

Because of their sensitivity to properties of the propagation medium, whistler mode signals are useful for the study of plasmas, especially those in space. For example, it is now known that whistler mode signals interact most strongly with the hot plasma when the waves are highly coherent. Accordingly, it is convenient to use the term "coherent wave instability" (CWI) as an operational description of the interaction. Since no full theory yet exists for the CWI, the theoretical modeling of this process is an important objective of plasma physics. The CWI is of interest to astrophysics as well because of the demonstrated prominence of similar phenomena in the magnetospheres of other planets in the solar system. In addition to its role in plasma physics, the CWI has applications to the control of radiation belts. Whistler mode waves may interact with resonant particle populations causing scattering of these particles out of their trapped orbits [*Inan et al.*, 1985]. The resulting precipitation deposits significant amounts of energy in the ionosphere, creating enhanced ionization, light, and X rays. The energy flux carried by the precipitated particles can exceed the electromagnetic flux of the whistler mode wave by several orders of magnitude. These effects demonstrate the importance to radiation belt physics of VLF waves injected from ground sources, such as lightning and VLF transmitters. Even the world's power grids have been found to influence the triggering and growth of magnetospheric VLF waves.

A method of remote sensing of the cold (i.e., thermal) plasma concentration is based on the dispersion properties of whistlers and VLF transmitter pulses [*Carpenter and Park*, 1973; *Carlson et al.*, 1985]. The energetic components of the plasma can be sensed through the amplification of the injected waves and the properties of the associated triggered emissions. Although the mechanisms of such interactions are not yet fully understood, it seems likely that the CWI could become a powerful new tool for the measurement of various parameters of the hot plasma population in the magnetosphere.

Another area to which the CWI can be applied is radio communication. One obvious use, which has yet to be developed in practical form, is the amplification in the magnetosphere of coherent VLF radio signals. It has been demonstrated that under appropriate conditions the power of VLF waves injected from the ground can be increased by a factor of 10^3 or more after passing through an interaction region near the equatorial plane. Another application relates to the background noise in the VLF band. Natural whistler mode signals such as chorus and hiss are generated at middle-to-high latitudes through interactions with energetic particles in the magnetosphere. Such signals often dominate the VLF noise spectrum in polar regions, both in the magnetosphere and on the ground below. The result is that the signal-to-noise ratio in a VLF communication circuit whose receiver is located in a polar region is often limited by naturally generated signals from the magnetosphere. In designing communication circuits for maximum signal-to-noise ratio it is important to know the distribution in time and space of natural background noise as well as its spectral form.

A further effect of the CWI on communications is the disturbance of radio circuits from ELF to HF by wave-induced particle precipitation in the D and E regions of the ionosphere. An example is the whistler-induced "Trimpi" effect, a sharp change in signal strength and phase over a period of less than a second followed by a 10–70 s recovery to predisturbance levels. Such perturbations can reduce the signaling efficiency of communication circuits and the accuracy of phase navigation systems [*Inan et al.*, 1985].

1.3. *Purpose, Scope, and Experimental Method*

The purpose of the experiments described in this paper is to determine the properties and generation mechanisms of whistler mode emissions in the magnetosphere. The experiments cover the frequency range from 1 to ~6 kHz and are carried out between Siple Station, Antarctica and its conjugate "area", including Roberval and Lake Mistissini, Quebec, as shown in Figure 1*a*. Input waveforms include CW, AM, FM, sideband, and noise simulations. Each signal format is repeated at appropriate intervals in order to remove temporal variations from the results. Observations at Siple Station of natural whistlers and emissions are used to locate the frequency band of maximum activity Formats include frequency ramps to aid in defining the propagation path. Key-up periods are introduced to reduce interference from echoes. The received signals are recorded on magnetic tape at the conjugate station. A stable pilot signal is also recorded with the Siple signals to permit recovery of the phase of the received signals.

1.4. *Why Antarctica?*

Siple Station, Antarctica, located at the base of the Antarctic peninsula, may seem an odd location at which to place a powerful (>100 kW) transmitter. Because of the considerable logistics expense in maintaining Siple Station, it is important that the reasons for this choice be understood. The first reason has to do with the fact that Siple

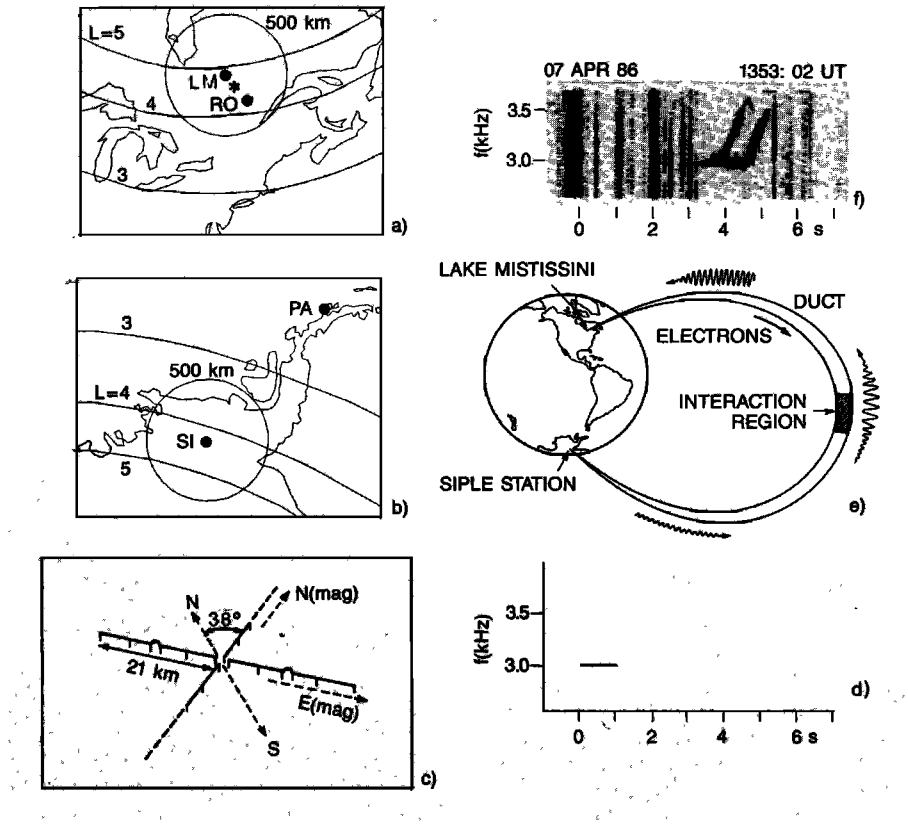

Fig.1. Elements of field-aligned whistler mode wave injection experiments between Siple Station, Antarctica (SI), and Lake Mistissini, Quebec, Canada (LM). A 1-s pulse (lower right) from SI is received at LM (upper right) after propagation along two ducts in which wave growth and triggering of rising emissions occurs. A VLF receiver located at Palmer (PA) provides data on low L shell whistler mode paths and on subionospheric propagation from Siple Station.

Station is located near the average position of the plasmapause ($L = 4$), a critically important boundary in the magnetosphere. It is here that the concentration of thermal electrons drops rapidly with radial distance by one to two orders of magnitude and where natural wave-particle interaction is prevalent. A second reason is the requirement that the conjugate point to the transmitter be readily accessible. The final, and perhaps most important, requirement is that radiation of the necessary power levels at these very low frequencies be economically feasible. At 3 kHz, a common operating frequency, the free space wavelength is 100 km. At most mid-latitude locations, where the ground is highly conducting, an antenna of the required size is difficult to build. To get reasonable efficiency (1–5%) from a horizontal antenna, it is necessary for the structure to be an appreciable fraction of a wavelength above the conducting ground. The thick (~2 km) Antarctic ice sheet provides enough elevation above the conducting rock for this purpose [*Raghuram et al.*, 1974]. It has been estimated that were the locations of the transmitter and the receiver to be interchanged, the power required from the transmitter would increase by roughly a factor of 100. The cost of equipment and fuel for such a facility would greatly exceed that for the present 150-kW transmitter. An alternate structure not requiring an ice sheet is the balloon-supported vertical antenna. Short-term experiments of this type have been successfully carried out between Alaska and New Zealand [*Dowden et al.*, 1978]. However, such experiments are limited to periods of good weather and the need to avoid interference with air traffic in the vicinity. For these reasons, only limited data have been obtained by this method.

To summarize, the primary requirements for these VLF wave injection experiments are (1) proximity to the plasmapause at $L = 4$, (2) an accessible conjugate point, and (3) adequate radiated power. Study of a world map, with ice thicknesses shown, reveals that West Antarctica uniquely meets all three conditions. The Greenland ice sheet is too high in geomagnetic latitude and there are no other significant ice sheets near $L = 4$.

The West Antarctic region where Siple Station is located has two additional advantages. The first is the low level of local noise resulting from the absence of thunderstorms on the Antarctic continent. The second is the high level of lightning activity in the conjugate region which provides many whistlers for comparison with man-made signals from the Siple transmitter. The whistler itself is used to measure path latitude and cold plasma concentration and furthermore plays a role in the generation of background noise such as hiss and chorus. Thus the natural phenomena that are prevalent at Siple Station add greatly to the value of that location.

The location of the Siple Station conjugate point is shown in Figure 1*a*. Two receiving locations are marked, one at Roberval and one at Lake Mistissini. The star represents the magnetic conjugate point to Siple Station as calculated for the year 1986 [*Stassinopoulis et al.*, 1984]. The conjugate point has been moving slowly to the northwest since the first experiments were made in 1973. Partly for this reason it has

been desirable to move the receiving location closer to the conjugate point as shown. A more important reason is the need to reduce interference from nearby power lines. The addition of new power distribution systems from Canada to the United States has raised the noise level at Roberval to a point where it is not possible to get good quality records at the lowest frequencies ($f \leq 3$ kHz).

1.5. *Satellite Observations*

An important component of the Siple wave injection experiments has been the support provided by various satellites, such as Explorer 45 (USA), IMP 6 (USA), EXOS-B (Japan), ISEE 1 (USA), ISIS 1 (Canada), ISIS 2 (Canada), and DE 1 (USA). Correlative data from these satellites have been used to determine the characteristics of the injected waves and energetic particles in the ionosphere and magnetosphere, and to establish the importance of coherent whistler mode waves to magnetospheric wave-particle interactions [*Bell et al.*, 1981, 1983*a*, *b*, 1985; *Inan and Helliwell*, 1982; *Kimura et al.*, 1983; *Sonwalkar et al.*, 1984; *Sonwalkar and Inan*, 1986; *Rastani et al.*, 1985]. A review of the observations of Siple signals by satellite is beyond the scope of the present paper, and the reader is referred to the above referenced works for details. A review of DE 1 satellite observations during Siple Station experiments can be found in a recent article by *Gurnett and Inan* [1988].

1.6. *Most Significant Results*

Perhaps the most significant finding thus far from these experiments is that signal growth increases as the signal bandwidth is reduced [*Helliwell et al.*, 1986*b*]. The mechanism of growth (CWI) exhibits at least seven distinct features, including (1) exponential temporal growth, (2) saturation, (3) emission triggering, (4) a threshold for onset of temporal growth, (5) suppression of growth by adjacent signals, (6) sidebands, and (7) entrainment. With few exceptions these properties can be measured only with controlled transmissions. The first hints as to the nature of the CWI were obtained from observations of Morse code signals from VLF transmitters which showed triggering by dashes (150 ms) but not by dots (50 ms). However the inability to control the frequency, power and modulation of these signals greatly limited such experiments. With the aid of the Siple transmitter, reproducible quantitative data on the nonlinear properties of the CWI have been obtained. Although the seven features noted above have been defined, their temporal behavior, their relations to one another, and their connection to the energetic particle distribution function have yet to be established. Thus there is much more to be learned from future experiments. In the meantime the available data are providing guidance to theoretical efforts aimed at modeling the observed processes. Current analytical and computer-based simulation models have been only partially successful in explaining the seven features listed above. Both experiment and theory will continue to play essential roles in the effort to reach a full understanding of the CWI.

1.7. *Plan of Paper*

The remainder of this paper is divided into four sections, including (1) the experimental method, (2) observations and their interpretations, (3) discussion of the main results and generalizations including comparison with theory, and (4) future directions for research. Mathematical details are omitted for ease of reading, but can be found in the references provided. It is intended that this paper constitute a topical review of these particular experiments with indications of where interesting problems exist and how they might be solved. An exhaustive review of the literature is beyond the scope of this paper.

2. EXPERIMENTAL METHOD

2.1. *Equipment*

The critical component of the CWI experiments is the transmitter. To meet the requirements of adjustable power, frequency, and modulation, an entirely new transmitter (called Jupiter) was constructed and placed in service in 1979. Surplus equipment from an Omega station provided the starting point for this transmitter, which includes provision for flexible modulation of two independent frequency synthesizers. Its predecessor, the so-called "Zeus" transmitter [*Helliwell and Katsufrakis*, 1978], which could only be modulated in frequency from a single synthesizer, provided data between 1973 and 1978.

A further improvement in the Siple Station facility was made in 1986, with the addition of crossed dipoles for the generation of variable polarization, depicted in Figure 1c. To provide for the excitation of the crossed antennas the Jupiter transmitter final amplifier was split into two parts, each with a push-pull output stage. These output stages are driven by separate exciters which in turn can be driven in common by one or two frequency synthesizers. One channel can be shifted in relative phase to permit the generation of any desired transmitted polarization. A photograph of the transmitter front panel as it now exists is shown in Figure 2. The functions of the transmitter are represented by a simplified block diagram shown in Figure 3. All modulation functions are under computer control.

The output of each transmitter channel is coupled to its antenna through an oil-filled output transformer together with appropriate tuning elements. Manually adjustable inductors and capacitors are used to set the resonant frequency of the antenna system to the center of the band of interest. Because of the relatively high Q of the antenna it is necessary to retune the antenna when the frequency is changed more than about 20% if a reasonable power output is to be achieved. In practice, the antenna power is close to maximum over a 500-Hz range centered on the resonant frquency as shown in Figure 4. The dashed curve shows the radiated power in decibels relative to an ideal antenna assuming the antenna is tuned to resonance. The three solid curves show the response of the antenna relative to the center frequency when the frequency is changed without altering the tuning. These three solid curves define the bandwidth of the antenna and determine the appropriate trade-off between power and bandwidth in sweep frequency experiments.

An important operational advantage of the crossed dipoles is that more power can be injected into the magnetosphere using right circular polarization. With linear polarization the antenna puts half of its power into the left-hand-polarized wave, which does not propagate in the ionized medium. Thus with right circular polarization the power

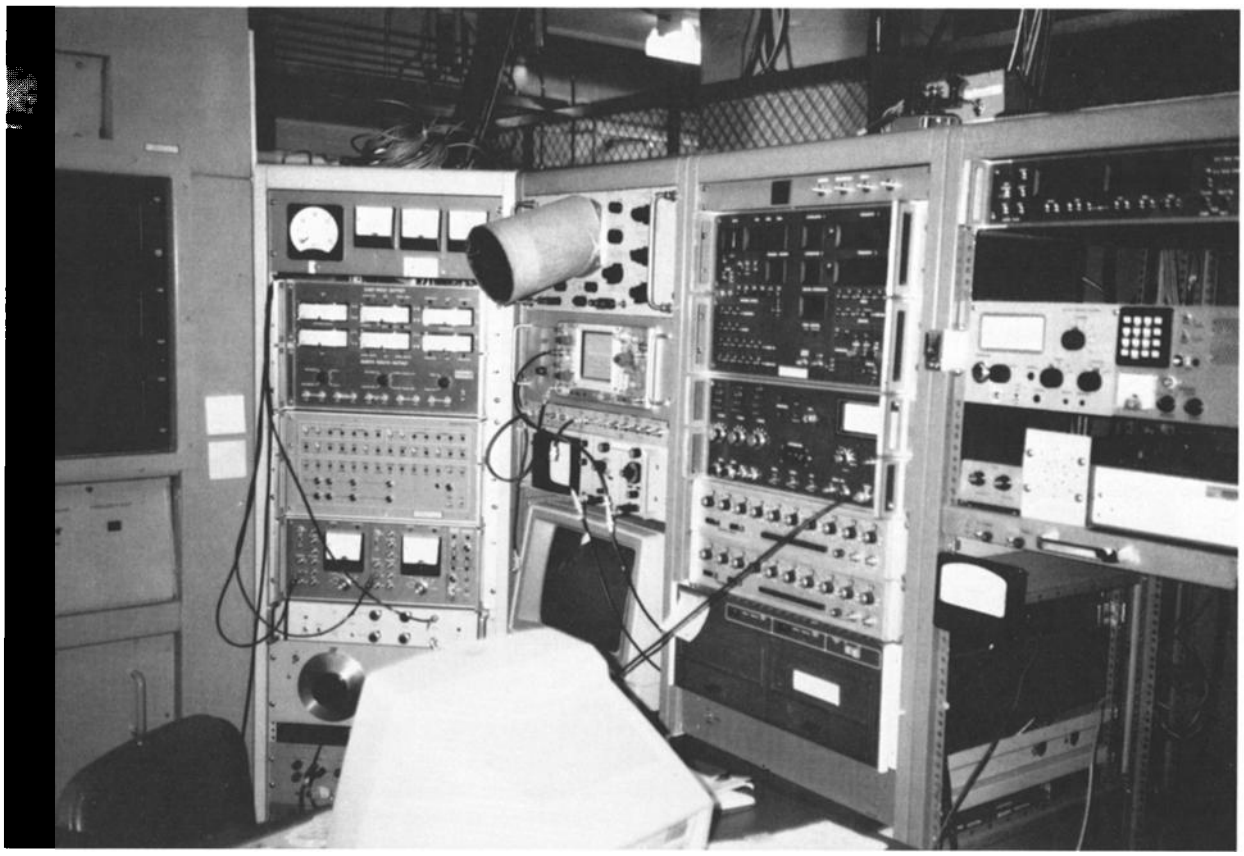

Fig. 2. Control panel of Jupiter stereo 150-kW transmitter.

that can be injected into the magnetosphere overhead is 3 dB (a factor of 2) greater than for a linear antenna.

An example of the response of the magnetosphere to left-hand and right-hand polarization is shown in Figure 5. In each case the transmission consists of a single carrier for the first second and two carriers for the second second. This combination was transmitted twice for each of the two circular polarizations. As shown in the sketch in Figure 5*d*, the left-hand polarization (looking up) will be attenuated in the ionosphere. Right-hand polarization will propagate without loss. Linear polarization would be transmitted with a 3-dB loss because half the power would go into the left-hand wave and half into the right-hand wave, accounting for the 3-dB advantage of right-hand over linear. Here we ignore the loss due to reflection at the relatively sharp lower boundary of the ionosphere.

The results of the right-hand/left-hand comparison are shown in Figures 5*a* and 5*b*. Here we see the onset of the

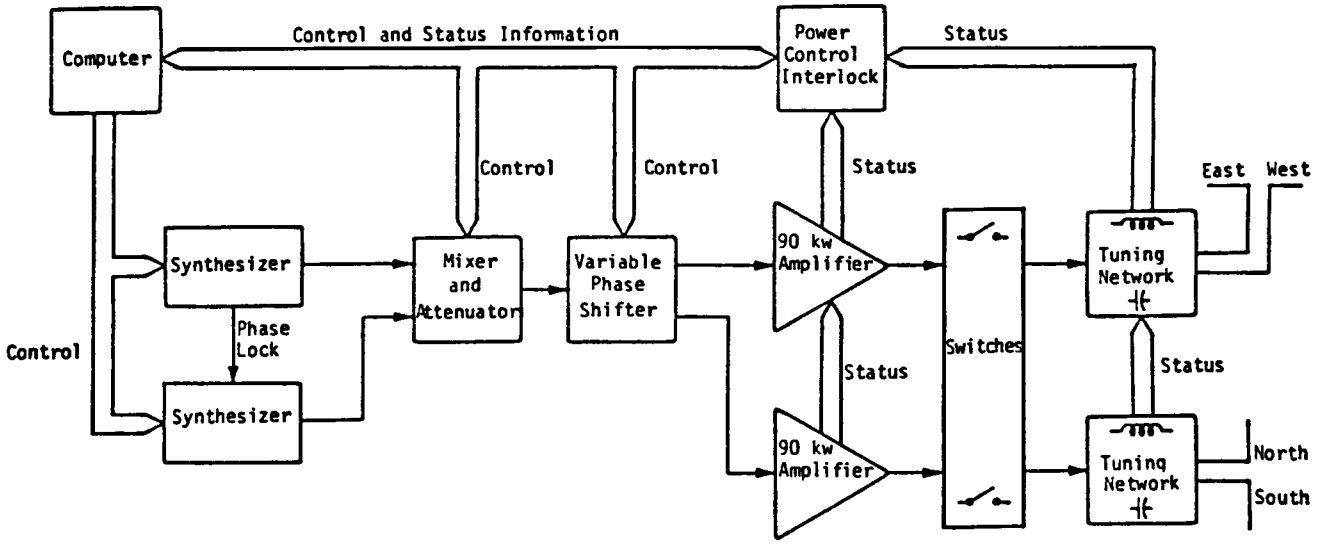

Fig. 3. Simplified block diagram of Jupiter transmitter components.

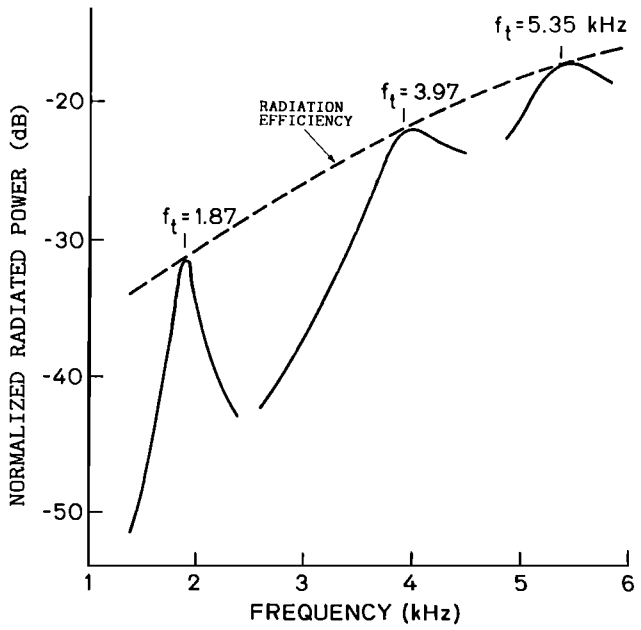

Fig. 4. Radiated power characteristics of the Siple VLF transmitter system (21-km dipole antenna). The solid curves show the estimated power radiated for three different resonant frequencies f_t, normalized by the power delivered to the antenna at each f_t. The dashed curve is the radiation efficiency [*Carlson et al.*, 1985].

signal, near $t = 2$ s, with an input intensity of about 17 dB for right-hand polarization. The input intensity for the left-hand polarization is close to the noise level and is estimated to be 4 dB. The difference, 13 dB, in the input strength, is in qualitative agreement with the predictions of magnetoionic theory. For the right-hand case the input signal is clearly above threshold as demonstrated by the roughly exponential temporal growth up to a saturation level of about 35 dB. Suppression of the saturation level of about 23 dB is observed when the upper carrier is turned on at 30 Hz above the lower carrier. Each pulse produces comparable results. For left-hand polarization there is no growth or triggering, indicating that the input level is below the threshold for growth.

An interesting aspect of multipath excitation by the cross is that as the power is increased more paths reach threshold and more total energy is injected into the magnetosphere. Wave-induced precipitation should therefore increase simply because more ducts have been excited above their thresholds. It has been found, for example, that the rms value of the output for right-hand polarization can be as much as 10 dB higher than that for linear polarization, as a result of the addition of more amplified ducted signals for the right-hand case.

The crossed dipole array is also used in the study of Earth-ionosphere waveguide propagation. For example, a constant amplitude linear polarization can be rotated in direction while observing the received intensity at Palmer, Halley, and South Pole [*Carpenter et al.*, 1988].

The receiving system is relatively simple compared with the transmitter and its antenna. At the receiver the main purpose of the antenna is to raise the external signal above the equipment noise level. The present system consists of two delta-shaped crossed loops mounted on a central 30-foot-high (~9 m) support with a base of 60 feet (18.3 m). These two mutually perpendicular antennas can be used for direction finding. In normal single-channel recording, one antenna is selected for minimum power line interference. A preamplifier at the base of the antenna boosts the received signal to an appropriate level for transmission to the recording equipment in the station. The receiving system includes provision for time marks, amplitude and frequency calibration, and automatic program control. In general, at most locations, it is necessary to provide either slot filters or low-pass filters to protect equipment against overload from powerful VLF transmitters. On the other hand, it is desirable to permit certain VLF signals to be recorded on the tape for their timing information. Normally, the transmitter and the receiver are kept synchronized to within 2–3 ms with the aid of a stable local frequency standard. However, in cases of doubt it is important to check the accuracy of relative timing between transmitter and receiver using independent sources such as WWV, Omega signals, or commonly recorded atmospherics.

Efficient analysis of the tape-recorded data requires a real-time spectrum analyzer. Its output is called a dynamic spectrum in which the amplitude is measured as a function of both time and frequency. To be effective, the dynamic analysis technique must employ filter bandwidths that are appropriate to the rates of change of frequency of the signals of interest. Thus flexibility in the choice of the filter bandwidth is needed. The two analog units that supply many of the illustrations shown in this paper are the Ubiquitous and Spectral Dynamics analyzers. Another spectrum analysis technique which is also used in some of the illustrations in this paper is based on the digital analysis of the tape-recorded analog data. The digital method, employing a fast Fourier transform, has the advantage of more flexibility in postanalysis processing and currently provides the only source of information on the phase of the signal.

Because of the limitations of dynamic spectrum displays of the type shown in Figure 1*f*, it is useful to be able to obtain the intensity as a function of time of an emission whose frequency changes slowly with time. This is done by using a tracking filter which follows the changing frequency of an emission so that its amplitude can be measured as a function of time. By combining the results from the tracking filter with those obtained simultaneously from the dynamic spectrum analysis, it is possible to obtain most of the important features of a transient signal.

2.2. *Methodology*

Although the experiments to be described in this paper are in some respects similar to fully controlled laboratory experiments, there are significant differences which must be taken into account. While the frequency, power, polarization, and modulation are specified by the experimenter, the parameters of the medium of propagation are variable and not controllable (at least at the present time). The ground-based experiments depend on the presence of suitable ducts (field-aligned enhancements of the thermal plasma), located at different latitudes and longitudes, which trap the input waves and guide them to the conjugate point where they can be received on the ground. Furthermore, since these are primarily active experiments, there must be enough energetic particles present in the magnetosphere to produce growth

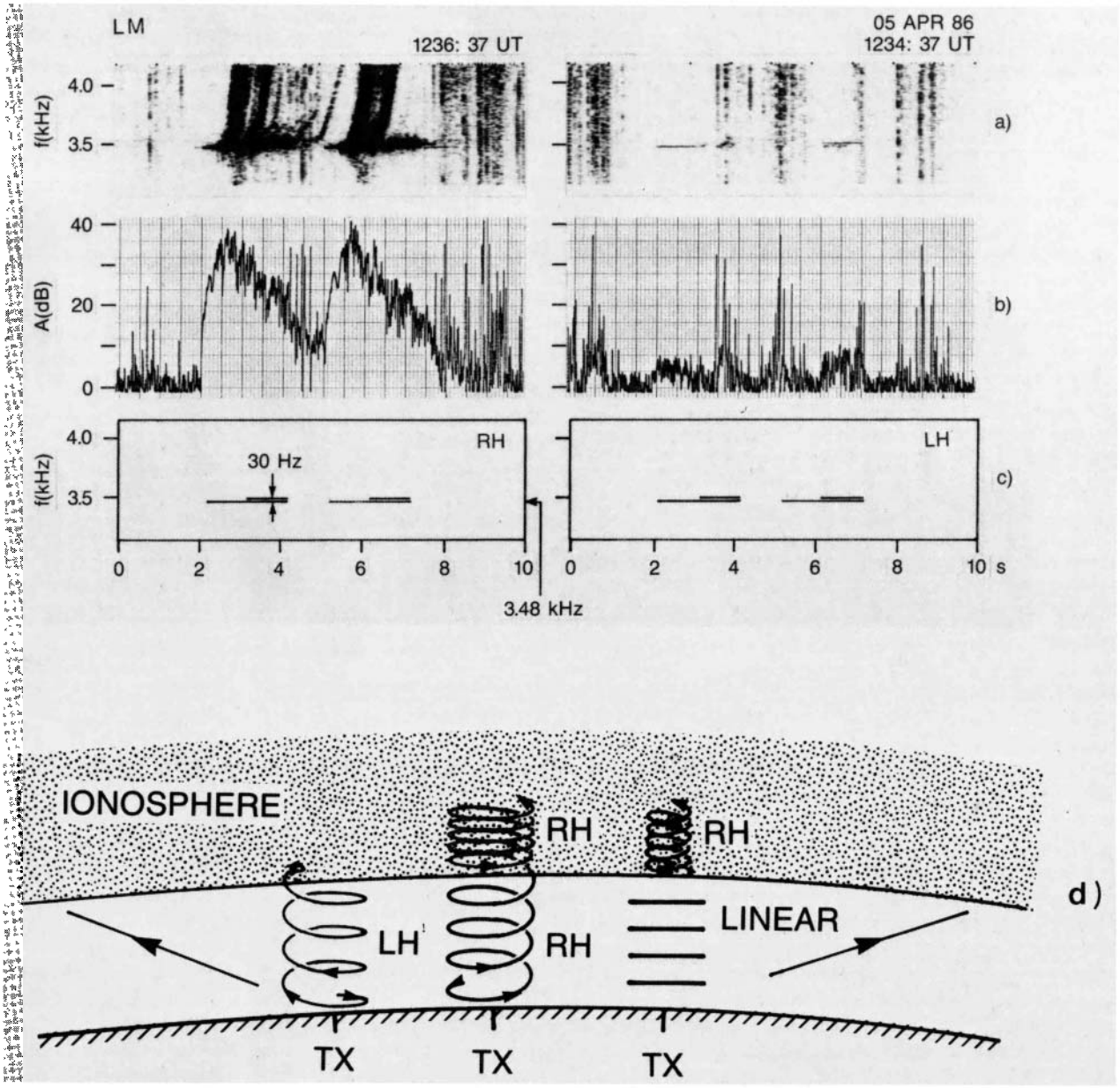

Fig. 5. Effect of transmitted polarization on whistler mode signals. (*a*) Spectra of signals received at Lake Mistissini, showing at left the magnetospheric response to right-hand-polarized signals and at right the response to left-hand-transmitted polarization. (*b*) Relative amplitude in dB within a 300-Hz band centered on the transmitted frequency of 3.48 kHz, showing a 30-dB difference in received signal level between the two polarizations. (*c*) Transmitted format, showing the use of a second signal to suppress temporal growth. (*d*) Diagram of the polarization experiment, and the conditions of overhead ionospheric excitation expected from theory.

and triggering. In addition, growth and emission triggering are believed to depend critically on the background noise level in the magnetosphere. As will be shown, the presence of other whistler mode signals, including those from the transmitter, can suppress growth of a test signal. If strong hiss and chorus are present, it may not be possible to radiate enough power to exceed the threshold for growth of the Siple signals. Thus the present experiments are critically dependent on timing as well as the choice of frequencies.

The optimum frequency range depends on conditions that vary with time. For ducts close to the transmitter (at $L = 4.3$) the most active frequencies fall in the range of 2–4 kHz. Sometimes the band of frequencies over which growth occurs is only a few hundred hertz wide. Thus it is necessary before carrying out an experiment to first find the active band and then to set the transmitter appropriately in frequency. As a general rule the two or three days of quieting following a significant magnetic disturbance provide good conditions for growth [*Carpenter and Bao*, 1983]. Experience shows that by using natural VLF emissions and K_p data as a basis for performing experiments, good results can be expected on 40–50% of the selected periods. Over a given year the number of days with excellent data may be a dozen or so and usable data may be obtained on many more. Thus the development of good criteria for selecting periods of transmissions becomes an important feature of experiment design.

Signal formats are tailored to each experiment. Wave-

forms include long and short single pulses, amplitude ramps, frequency ramps, and multifrequency signals. Formats must be repeated enough times to remove the effects of temporal variations. Other requirements include avoiding the effects of echo suppression and multipath. Echo suppression occurs when the echo of one transmitted signal passes through the interaction region at the same time as the next test pulse. The echo generally suppresses the growth of the new signal when their frequency separation is less than 100–200 Hz. In order to eliminate or minimize echo suppression, the duration of the test signal is limited to 5 s and is not repeated on the same frequency for another 7 s, giving a total cycle time of 12 s. During the 7-s off period the transmitter signal may be moved to a second frequency such that its echoes do not interfere with the primary signals on the first frequency.

Multipath effects are more difficult to control. There may be four or five, or more, paths excited simultaneously by a single pulse producing four or five separate echoes at the receiver, each exhibiting different growth, saturation, and triggering behavior. An effective way to minimize interference between signals on different paths is to use frequency ramps, with slopes high enough to separate the individual paths. Frequency slopes of 1–2 kHz/s are commonly used. At higher slopes the signals show reduced growth and triggering. For single-frequency experiments where the growth rate, the saturation level, and the triggering properties are important, the best situation is a single path or one prominent path on which the signals are much stronger than on other competing paths.

An interesting aspect of formatting relates to the so-called threshold effect, which is the signal level above which growth and triggering can occur. Generally speaking, each path has its own threshold, which can vary with time. Thus it is possible to set the transmitted power such that only one path exhibits growth and triggering. However, this condition is not readily achieved with the present technology because of the personnel and time required to relay information from the conjugate point back to the transmitter. Ideally, a satellite link would transmit the received signals back to Siple Station in real time, allowing the operator to manually adjust the transmitter power output to eliminate all but one path. This is a highly desirable objective for future controlled experiments

The scheduling of formats is an important factor in obtaining good data. Generally, it is desirable to obtain at least three independent samples of each measurement. On the other hand, since the unusually good days occur rather infrequently, it is useful to bundle formats into packages so that several experiments will be performed together on a good day. Thus there is a trade-off between the number of repetitions of any one experiment and the number of experiments that will be run during an active period, which typically lasts for 2–3 hours.

The method of experimentation described above applies mainly to ground observations at the conjugate point. Other experiments involving subionospheric propagation and transmissions to satellites have somewhat different requirements. For subionosphere transmission the conditions are much less restrictive and are related mainly to the degree of magnetic disturbance and the time of day. Transmissions to satellites, on the other hand, are highly orbit dependent and are scheduled on the basis of proximity of the satellite to the transmitter as defined by the ray path. Real-time control of the transmitter based on observation of the spectrum telemetered from the satellite to the ground is highly desirable. This technique has been developed as part of the Siple Station DE 1 satellite program. It has permitted the transmitter frequency to be set optimally with respect to in situ noise bands which reduce the signal to noise ratio.

3. Experimental Observations And Their Interpretation

Because the results in these experiments depend on the spectrum of the transmitted signal, they have been grouped according to modulation format. In the first group are the single-frequency step function pulses of roughly 50 ms or greater duration. Second are step function signals in which the frequency varies slowly with time, as in a frequency ramp. In the third group, multiple frequencies are transmitted simultaneously in the form of amplitude modulation, frequency modulation, or two or more independent carriers added together A subset of the third category is noise simulation in which random noise is approximated by means of an FM transmission with randomly chosen sequential frequencies.

3.1. *Single-Frequency Behavior*

A step function single-frequency pulse may produce exponential temporal growth, saturation, and triggering, as shown in Figure 1*f*. If, however, the radiated power is reduced below a critical value, both growth and triggering cease. The critical level is called the "threshold" for the onset of growth. It is a fundamental property of the coherent wave instability and determines the transmitter power required to carry out experiments on the CWI. An example of the threshold effect is shown in Figure 6*b*. Here a 3-s pulse begins at 30 dB below peak value, ramping up to full power 1.5 s later, as shown by the solid curve in Figure 6*b*. The received signal, shown by dots, at first follows the transmitted intensity except for a periodic pulsation in its intensity at a frequency of about 8 Hz. (This effect is attributed to the beat between the received Siple pulse and a local power line harmonic.) As the transmitted amplitude approaches its peak value, the slope of the received amplitude abruptly increases to 110 dB/s, reaching saturation after 23 dB of growth. Just after saturation is reached, the signal trace broadens in frequency (see Figure 6*a*), and the average frequency begins to rise rapidly with time. The frequency of this triggered "riser" reaches a maximum value of 4.7 kHz and then starts to fall just before it abruptly terminates. In the meantime the signal from the carrier filter, shown in Figure 6*b*, falls to a value below the unamplified level, which is just above the threshold. In about 100 ms it recovers to the unamplified level, after which it grows at the same rate (110 dB/s) as before, reaching the same saturation level as before. This process is repeated again, giving three sequences of exponential growth, saturation, and triggering. The fourth riser is attributed to an additional triggering event caused by termination of the applied pulse.

A key feature of growth and triggering in single-frequency experiments is the phase behavior shown in Figure 6*c*. (Each of the sharp jumps in the phase up to ~1.5 s is the result of a sferic (seen on the top panel as a vertical line) that resets the phase reference.) As the threshold is crossed at ~1.7 s, the phase begins to advance parabolically with time,

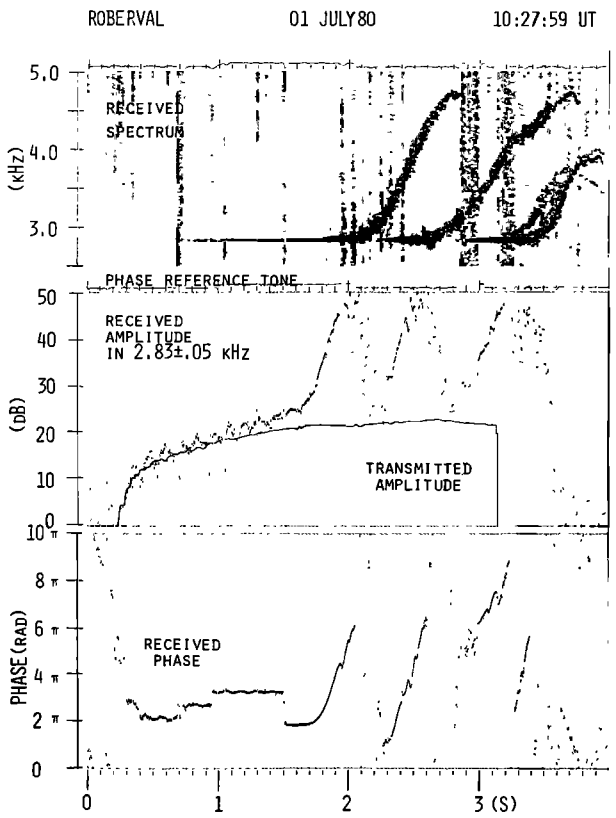

Fig. 6. Threshold effect. (*a*) Dynamic spectrum of a 3-s pulse transmitted from Siple Station and observed at Lake Mistissini. (*b*) Amplitudes of transmitted pulse (solid line) and received pulse in a 100-Hz bandwidth centered on carrier at 2830 Hz. (*c*) Phase of received signal; phase jumps are caused by sferics (vertical lines in Figure 6*a*) that perturb the local phase reference signal [*Paschal and Helliwell*, 1984].

corresponding to a linear increase in frequency of ~35 Hz/s. Just after saturation is reached, the phase (and frequency) rise more rapidly, and the emission is said to have begun. (Prior to this point, the stimulated component of the signal is sometimes referred to as an "embryo" emission [*Dowden et al.*, 1978].) Phase advance, in general, accompanies temporal growth of the signal but has not yet been predicted in any published theory.

The effect of the threshold on multipath growth and triggering is illustrated in a different way by Figure 7. The format shown at the bottom of the figure is transmitted at different power levels which are held constant throughout each transmission. A peak power of 24 kW is transmitted in the top panel; multipath propagation is seen on both the rising and the falling ramps, with four paths being readily apparent. As the power input is decreased, the width and complexity of the received signal pattern decreases corresponding to progressive dropouts of the weaker paths. Thus at 1.5 kW all paths but one have dropped out. At 0.6 kW there is no temporal growth and no triggering of emissions on any path, only a reproduction of the applied signal. Thus the transmitter power threshold for growth on the most active path must lie between 0.6 and 1.5 kW. The actual transition from zero to full growth rate is best defined by the amplitude ramp of Figure 6 and is about 2 dB. It has been suggested that the threshold effect is the result of the applied signal being too weak to control the phase bunching process in the presence of the in situ background noise [*Helliwell et al.*, 1980].

Saturation is usually accompanied by broadening of the spectrum and often by a band-limited impulse (BLI), as shown in Figure 6, just before the second triggered riser. However, when the signal terminates before triggering occurs, it is usually observed that in addition to a BLI a falling tone is triggered at the end of the pulse (e.g., Figure 19). Such emissions are described by the term "end-triggering" or "termination triggering". In virtually every case of end triggering, the frequency first rises rapidly, reaching an offset of up to 100 Hz. It may then continue to rise, more slowly, but usually holds constant for a brief period and then falls.

Another form of end triggering occurs when a gap is inserted in a constant frequency pulse. An example is shown in Figure 8 in which a 10 ms gap was introduced at 400 ms into a 1-s-long pulse. A BLI and one or two risers are created in the gap. These risers start close to harmonics of the Canadian power grid, at 5.1 kHz and/or 5.16 kHz. It is noteworthy that no falling tone was generated as is usually the case at the end of a pulse. On the other hand, the BLI closely resembles the BLIs that occur at the end of a pulse. It is postulated that the mechanism for the BLI is the same in both cases but that the frequency change of the continuing emission is affected by the presence or absence of the carrier signal at the end of the 10-ms gap.

The effect of gap duration on end triggerring is illustrated in Figure 9, where the gap duration is varied from 10 to 130 ms. Each gap excites a perturbation but no falling tone occurs until the gap duration equals or exceeds 100 ms. For shorter gaps the emission is unable to pass through the gap because the carrier reappears too soon, entraining the emission as it attempts to cross the carrier frequency.

3.2. *Frequency Ramps*

A phenomenon called second-order resonance has been invoked to explain the growth of coherent waves. An electron is in second-order resonance at the point where the second time derivative of the phase of its perpendicular velocity with respect to the wave fields is zero. This point has been called the "phase equator" [*Helliwell and Inan*, 1982]. It has been found that when the frequency of the applied signal is slowly varied, the condition for second-order resonance still applies (with certain restrictions) if the phase equator is shifted appropriately in latitude [*Helliwell*, 1970; *Carlson et al.*, 1985]. The reason for this behavior is that the parabolic increase in gyrofrequency with latitude for low pitch angle particles causes the Doppler-shifted wave frequency as seen by these particles to be related to the local gyrofrequency in the same way at all locations regardless of df/dt as long as the latitude and the pitch angle are both small. For example, a 1-kHz/s ramp shows roughly the same growth and triggering properties at a point (the phase equator) about 2000 km downstream from the magnetic equator as a constant frequency ramp shows on the magnetic equator. Because growth generally varies with frequency, the conditions may not in actuality be the same. Also, the resonant electron energy increases with latitude, usually causing some reduction in growth rate.

Frequency ramp behavior is shown schematically in Figure 10. The transmitted signals, both rising and falling, are

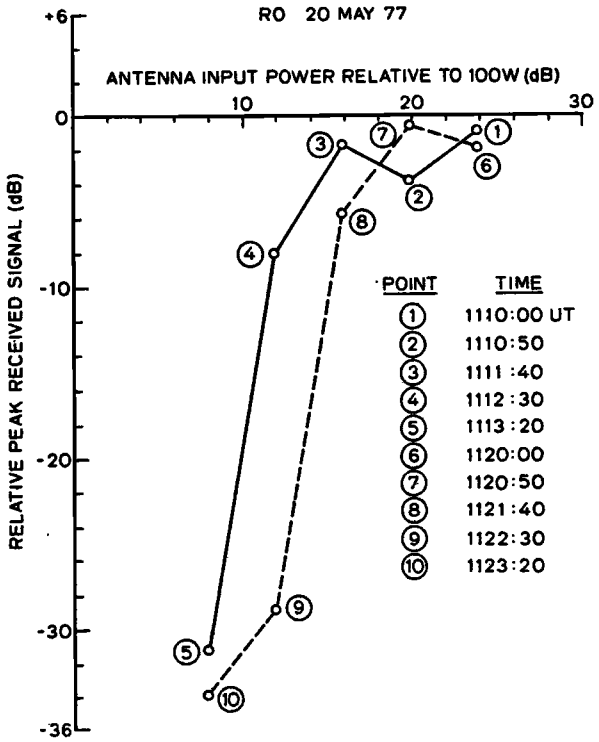

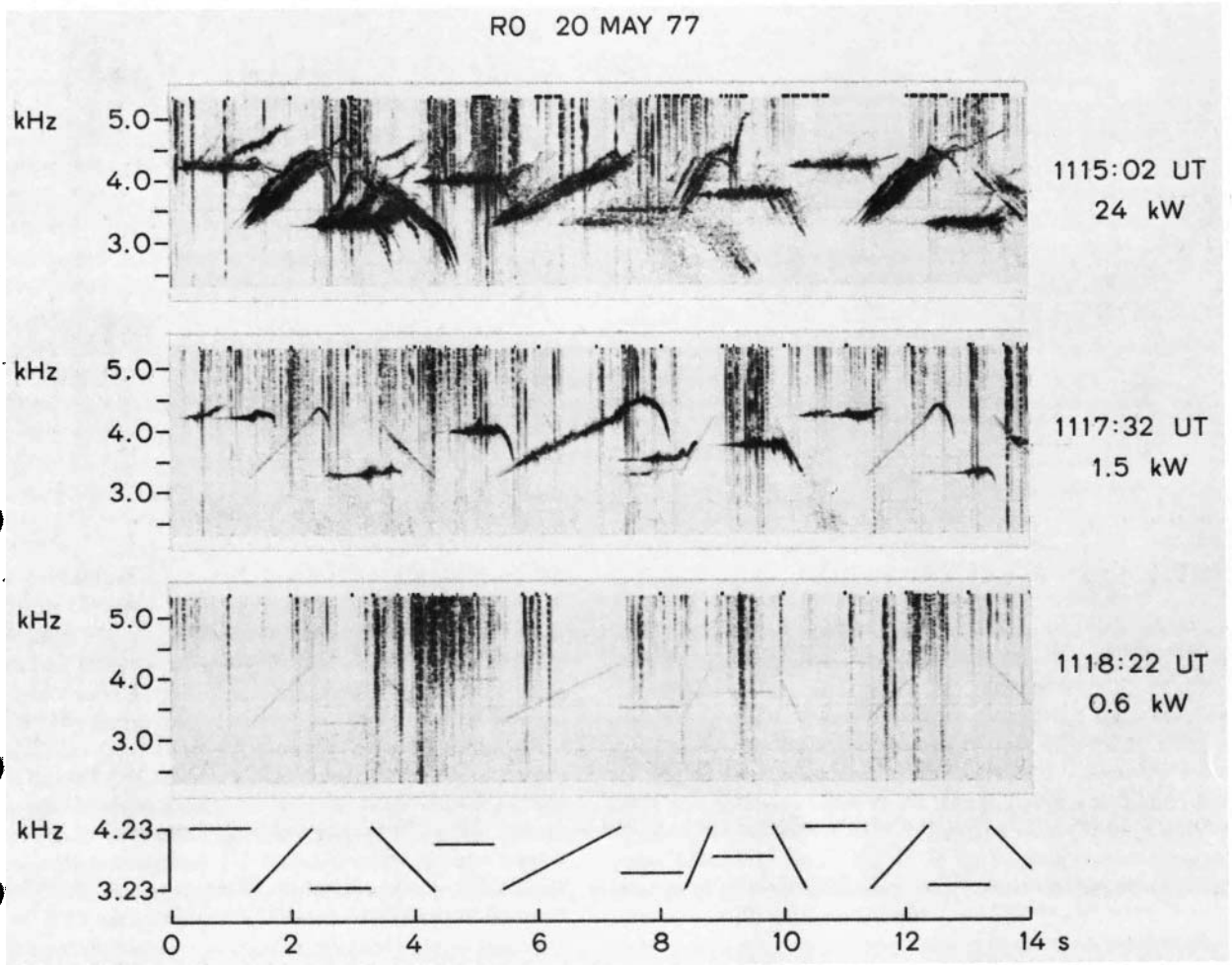

Fig. 7. Multipath threshold. Lowest panel shows format of transmitted signal. The response at Roberval to successive decreases in transmitted power is shown in the upper three panels. At 24 kW, four paths are above threshold; at 1.5 kW there is only one; and at 0.6 kW there are none [*Helliwell et al.*, 1980].

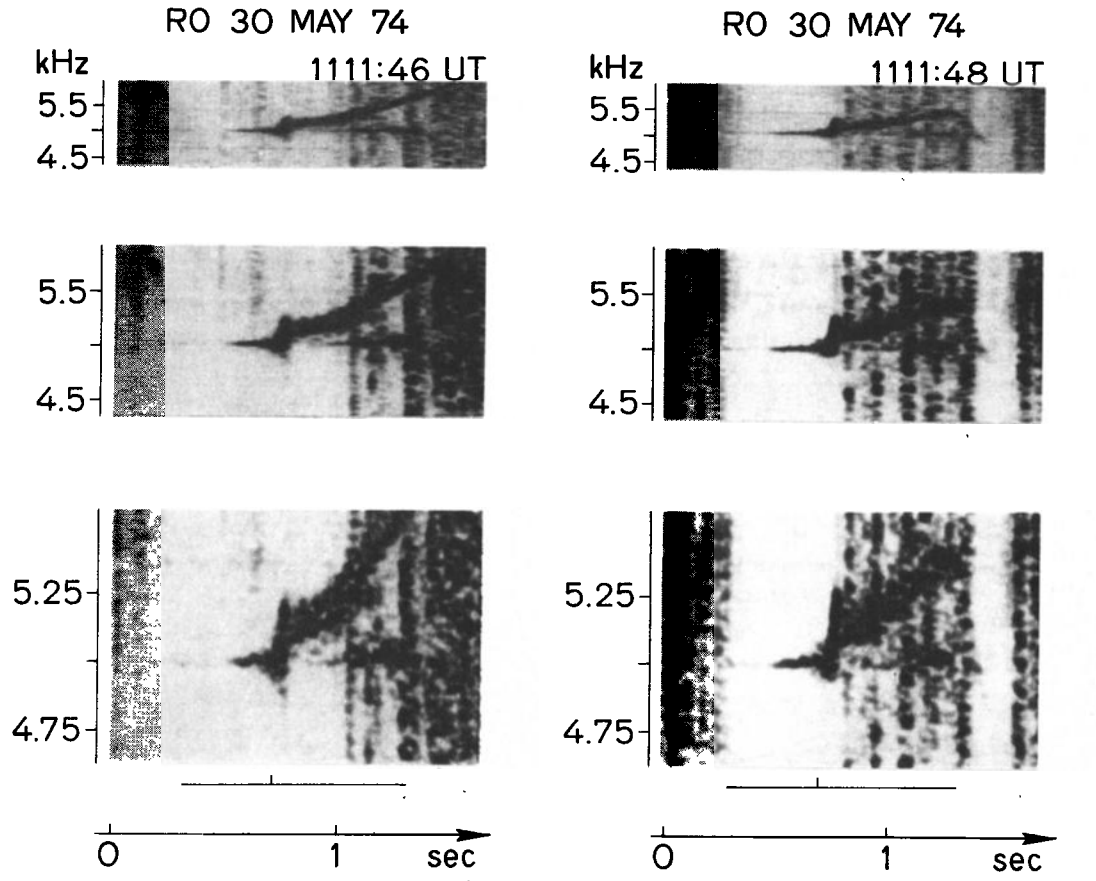

Fig. 8. Gap-induced emissions. A 10-ms gap introduced at 400 ms into a 1-s pulse, as shown by the transmitted format at the bottom of each vertical panel, triggers BLIs and rising emissions. Two events are shown, 2 s apart, to demonstrate repeatability. Each event is displayed in three frequency ranges to illustrate the $f - t$ structure. Rising emissions begin in the BLI at the 85th (5.1 kHz) and/or the 86th (5.16 kHz) harmonic of the Canadian power grid [*Chang and Helliwell*, 1979].

shown in the upper left, below which are the received signals as they would be dispersed in a model magnetosphere. The slower ramps show triggered emissions which rise above the frequency of the exciting signal and reach approximately the same cutoff frequency. The faster ramps generally are weaker at the receiver, and their f–t traces show more pronounced evidence of dispersion. The circled numbers on the diagram, 1-5, indicate dispersion, lower cutoff, saturation, emissions, and upper cutoff, respectively. The upper cutoff, in many cases, is associated with a ducting property of field-aligned enhancements of the thermal plasma in which whistler mode energy is trapped only at frequencies below one-half the local gyrofrequency [*Helliwell*, 1965]. Thus signal energy above half the minimum gyrofrequency along the path will become detrapped, in most cases, and hence will not be received at the ground. Exceptions, called "super whistlers", are sometimes seen near the plasmapause [*Bernhardt*, 1979].

Illustrating the idealized ramp relationships described above is the set of observed spectra shown in Figure 11. The slower ramps show the most growth and triggering of emissions. It will be noted that the triggered risers reach about the same maximum frequency, close to the duct cutoff frequency. As the ramp slope increases in magnitude, both growth and triggering decrease. The decrease in apparent intensity of a fast ramp is partly associated with its short duration (not enough time for growth to occur), but it is also dependent on the growth rate. Theoretically, this can be explained by the fact that as the region of second-order resonance moves away from the equator, the velocity of the resonant electrons increases. The electron energy then rises, and for the usual electron distribution function the number density falls off markedly. The result is fewer energetic electrons to provide growth.

The quantitative relations for second-order resonance for linear ramps are given in Figure 12. These curves show frequency versus latitude of the phase equator, parametric in ramp slope. It is assumed that the resonant electrons have a 30° pitch angle. For small slopes and points near the equator it is seen that the latitude of second-order resonance is approximately proportional to the slope of the emission. However, for high slopes the relationship is more complex, as the curves illustrate.

As in the fixed frequency case, slow ramps generally show a period of growth followed by saturation and triggering, as shown in Figure 11. In the top panel we see that triggering occurs only for slope magnitudes of 0.5 kHz/s or less. For the –1 kHz/s ramp there are no triggered risers, but growth still occurs, extending down to an unusually low frequency, ~2 kHz. (transmitted slope ramp covers 1–8 kHz.) Why does this particular ramp reach a lower frequency than any other on the record? The answer may be that at this partic-

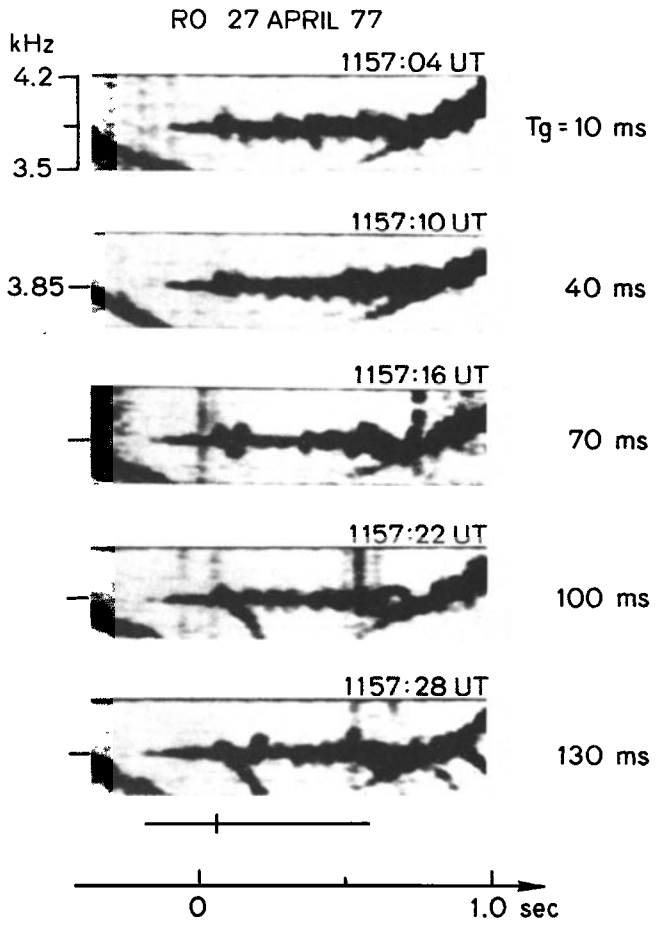

Fig. 9. Effect of gap duration on triggering. A gap is started at the 250th ms of a 750-ms pulse; its duration $T_g = 10, 40, 70, 100$, and 130 ms, as shown. Emissions are either suppressed or entrained by the carrier for $T_g = 10$ to 70 ms. For $T_g \geq 100$ ms, a faller is triggered as in ordinary end-triggering events [*Chang and Helliwell*, 1979].

ular slope, the phase advance of the emission energy was not sufficient to produce a triggered emission, and consequently, the amplified signal was able to remain phase-locked to the applied ramp. The measured amplitude of the −1 kHz ramp is shown in the top panel of Figure 13. Also shown is the predicted relative radiated power profile based on the calculated efficiency of the antenna as a function of frequency, taken from Figure 4. At 2 kHz there is a discontinuity in the frequency trace indicating the triggering of a faller which is well defined down to a frequency of ~1.6 kHz.

One of the interesting features of this particular event is the relation between the peak output signal and the estimated input signal, the ratio of which reaches a maximum of ~55 dB. The corresponding input signal strength at the equator is estimated to be 10^{-3} pT. Even at such a low field intensity, phase-locked growth is maintained, indicating that spatial growth of the order of 20–30 dB can occur in the magnetosphere at very low input signal levels. There has been controversy in the literature as to the level of input signal required to excite the CWI [*Matsumoto et al.*, 1980]; the data of Figure 13 provide evidence that nontrapped particles must be included in any model of the CWI. Models based on resonant electron trapping typically require signal levels at the input to the interaction region of >1 pT, three orders of magnitude greater than the minimum input field estimated for Figure 13. It may be the case therefore that any input signal can excite the CWI, provided only that the input signal exceeds the threshold value set by ambient noise.

3.3. *Multifrequency Experiments*

It has been stated that growth occurs preferentially on narrow-band signals. To determine the relationship between signal bandwidth and growth a series of experiments was performed in which the spectrum of the transmitted signal was broadened in different ways [*Helliwell*, 1983*a*, *b*]. The methods included amplitude modulation (AM), frequency modulation (FM), and sideband modulation (S), meaning the use of two independent carriers closely spaced in frequency. To provide an overall assessment of the output from such a multifrequency signal, the three types of modulation were applied so as to produce comparable spectra, an example of which is shown in Figure 14*a*. For AM, modulation was 100%, and for FM the modulation index was set to unity. In the case of sideband modulation the two carriers were equal in magnitude. At the conjugate point the rms output for each of these three cases was measured, as shown in Figure 14*b*. Minimum output occurs at $\Delta f = 20$ Hz, independent of the type of modulation. This result shows that the frequency spacing, not the form of the transmitted modulation, is the primary factor in growth. However, we should note that dispersion alters the phasing among the sidebands, causing conversion of AM to FM and vice versa [*Chang and Helliwell*, 1980].

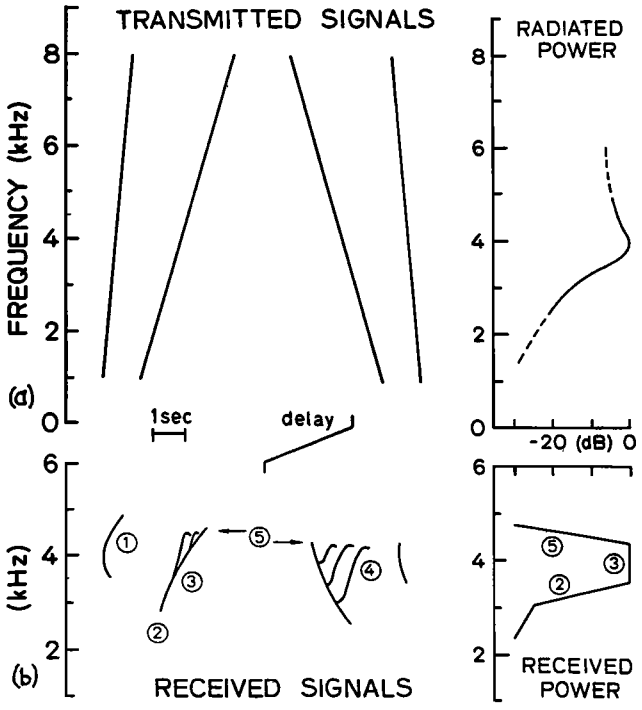

Fig. 10. Sketch of $f-t$ spectra of ramps and associated risers. (*a*) Rising and falling transmitted ramps and radiated power profile (right). (*b*) Received ramps and emissions; circled numbers, one through five, indicate dispersion, lower cutoff, saturation, emissions, and upper cutoff, respectively [*Carlson et al.*, 1985].

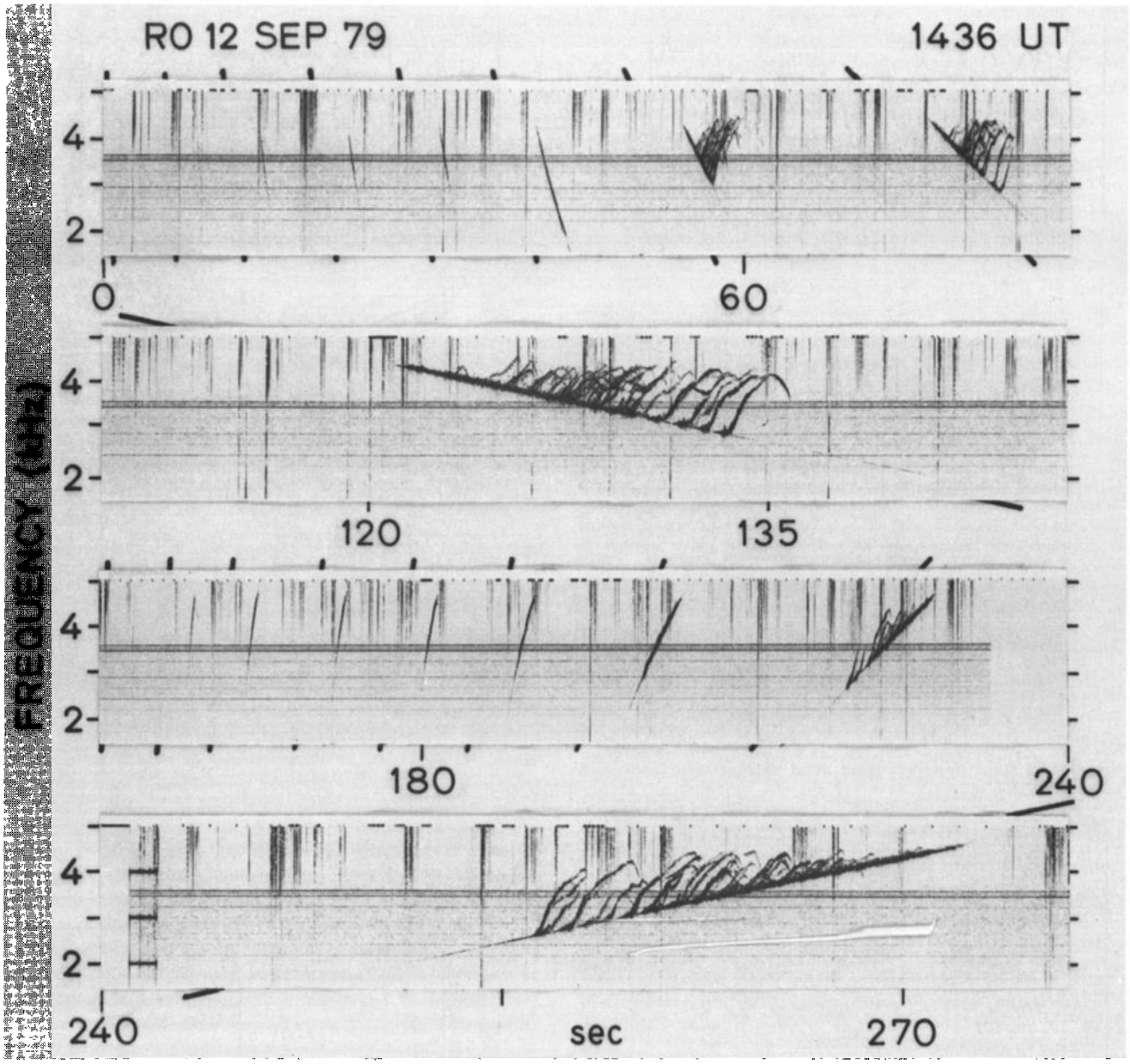

Fig. 11. Spectra of VLF ramps received at Roberval. Ramp slope magnitudes vary from 7 to 0.125 kHz/s. Sloping tick marks along borders of the panels define the transmitted slopes [*Carlson et al.*, 1985].

An interpretation of the growth-bandwidth curve of Figure 14*b* in terms of second-order resonance can be developed by considering both time and frequency domains for the sideband, or beat case. At small Δf each beat is relatively long. For example, at 10 Hz the beat duration is 100 ms, which is comparable with the entire growth time of a single frequency pulse for high growth rates. On the other hand, for a frequency separation of 50 Hz the duration of the beat is 20 ms, which is short compared with either the growth time or the transit time of an electron traversing the interaction region [*Helliwell and Inan*, 1982]. Thus for Δf less than 10 Hz each beat should approach its saturation amplitude, in agreement with the data. At the higher Δf values the growth of each beat viewed in the time domain is too small to be of importance. As Δf increases, each spectral component has access to a wider range of parallel velocities of electrons that are unperturbed by the other component and can therefore approach its unperturbed maximum amplitude. For $\Delta f > 100$–200 Hz there is little interaction between the adjacent components each of which reaches its single-frequency saturation value.

To determine the temporal properties of suppression, we perform another experiment, called line coupling (LICO). Two constant amplitude carriers of equal intensity are transmitted at different frequency spacings, with one of the carriers being switched on and off, as shown in Figure 15. In the top panel the two carriers are spaced 30 Hz apart, and they fade slowly in amplitude, as defined by the lower two lines in the spectrum. There is little or no growth of the carriers. The upper line is a sideband created by nonlinear interaction between the two input waves, and its fading can be seen to differ from the fading of the two injected carriers.

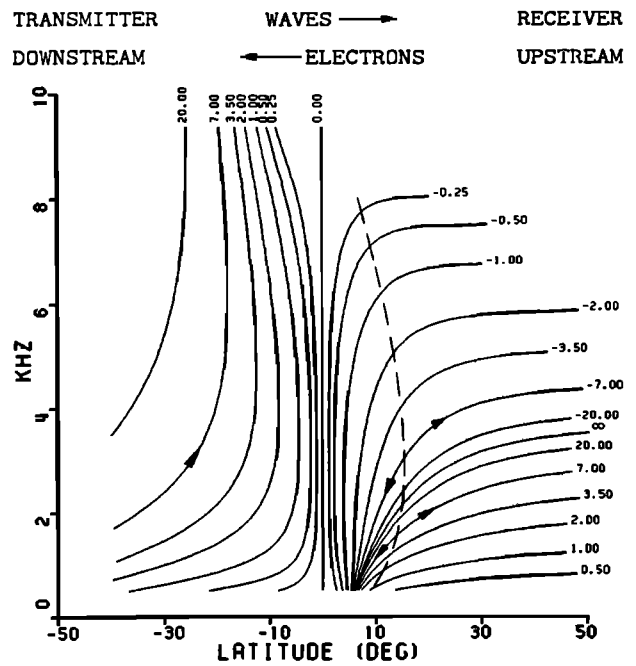

Fig. 12. Second-order resonance relations, showing frequency versus the magnetic latitude of the phase equator (center of interaction region), parametric in ramp slope. Arrows indicate directions of changes with time. Dashed curve marks focus of frequencies and latitudes where the phase equator splits into two branches, one moving up in frequency with time and the other moving down. A 30° pitch angle is assumed [*Carlson et al.*, 1985].

This circumstance is explained in terms of multipath interference, a common effect in these experiments. The second panel from the top shows the rms amplitude with its 30-Hz beat pattern between the two carriers clearly defined.

An important feature of the LJCO experiment is the recovery from suppression that occurs when the upper carrier is turned off at ~55 s. The lower carrier immediately grows to saturation, roughly 20 dB above its unamplified value; triggering of risers then begins. This experiment shows that recovery from suppression is essentially instantaneous, to an accuracy of 10–15 ms.

As frequency separation is increased, the coupling between the two components is reduced, as shown in the bottom two panels of Figure 15, where the frequency spacing is 60 Hz. In this case the upper component shows distinctly greater intensity and more triggering than the lower component. A weak upper sideband also is seen as in the previous case. Such asymmetry in mutual suppression, which occurs for the larger frequency spacings (e.g., $\Delta f = 60$ Hz), is a characteristic of these experiments. When the upper signal is turned off, the lower-frequency signal again immediately begins its return to the normal unperturbed level, as shown by the amplitude record in the lower panel. There is a residual line at the frequency of the upper carrier which is attributed to echoing of the signal on the upper frequency. The difference in rms intensity of ~10 dB between the two-frequency ($\Delta f = 60$ Hz) segment and the single-frequency segment is comparable to what was observed in the modulation experiment illustrated in Figure 14.

The effect of frequency spacing on sidebands and growth is further illustrated by varying the frequency spacing while keeping the two components at the same intensity, as in Figure 16. For $\Delta f < 12$ Hz, peak intensity reaches a relatively high value, and sidebands appear up to seventh order. Such high intensity suggests coupling between the emissions of each beat such that each emission reinforces the next one, possibly as the result of favorable phasing between the end of one emission and the beginning of the next. For $\Delta f > 12$ Hz, the peak output falls rather abruptly, suggesting that the time between beats was inadequate to develop the required phase advance for coherent coupling between adjacent emissions. Fluctuations in the amplitude of the beat for $\Delta f > 12$ Hz is attributed to multipath fading.

A second feature of two-frequency interaction is the effect of changing the intensity ratio of the two carriers; an example is shown in Figure 17, where $\Delta f = 20$ Hz. In Figure 17*a*, two pulse sequences provide calibration for the experiment. In the first a step function single frequency signal produces exponential growth, saturation, and triggering. One second later a second signal of equal amplitude is turned on 20 Hz below the carrier, as shown in the bottom panel of Figure 17*a*. After the emissions damp out, the unamplified output of the beat is clearly seen. This same sequence is repeated in reverse beginning at 6 s. First we see the unamplified beat pattern, similar to that at the tail end of the first segment. When the lower-frequency component of the doublet is turned off, the remaining component grows to saturation and triggers emissions.

The variable amplitude ratio experiment is shown in Figure 17*b* where the lower-frequency component is ramped up in amplitude in the first second at the rate of 20 dB/s and down in amplitude at −20 dB/s in the last second of the sequence. In the first sequence, where the lower frequency component ramps up in amplitude, there is substantial growth at the upper frequency which saturates at 7 dB below the peak value in Figure 17*a*. At an amplitude ratio of ~ 12 dB, and shortly after the peak of the total output is reached, there is a maximum in sideband generation, with both first- and second-order sidebands appearing both above and below the input carriers. The same sequence is repeated on the down ramp except for a time delay. Thus it appears that sideband generation is maximized when the ratio of the two input signals is of the order of 12–15 dB. As sidebands grow, they beat with one another, generating more sidebands. These sidebands in turn tend to suppress growth at the carrier frequencies. However, if one of the two carriers is weaker than the sidebands themselves, it will be amplified as shown in Figure 17*b*. Empirically, we see that sideband amplitudes are maximized when both growth and beat modulation are simultaneously present.

A mechanism for the generation of sidebands can be deduced from high time resolution spectra of the beats, such as the experiment shown in Figure 18. Sidebands are produced by the beat between two frequencies 20 Hz apart. As the response time is reduced by increasing the filter bandwidth, the time domain sequence of events is revealed. For a filter bandwidth of 80 Hz short emissions appear between adjacent beats. The magnitudes of these "interbeat" emissions can be measured by analyzing the same data with a filter that gives the amplitude in a bandwidth of 300 Hz, as shown in the bottom panel. Here we see the classical beat pattern modulated by short interbeat emissions which have intensities that are typically 6 dB below the intensity of the beats themselves. It is these interbeat emissions, whose frequen-

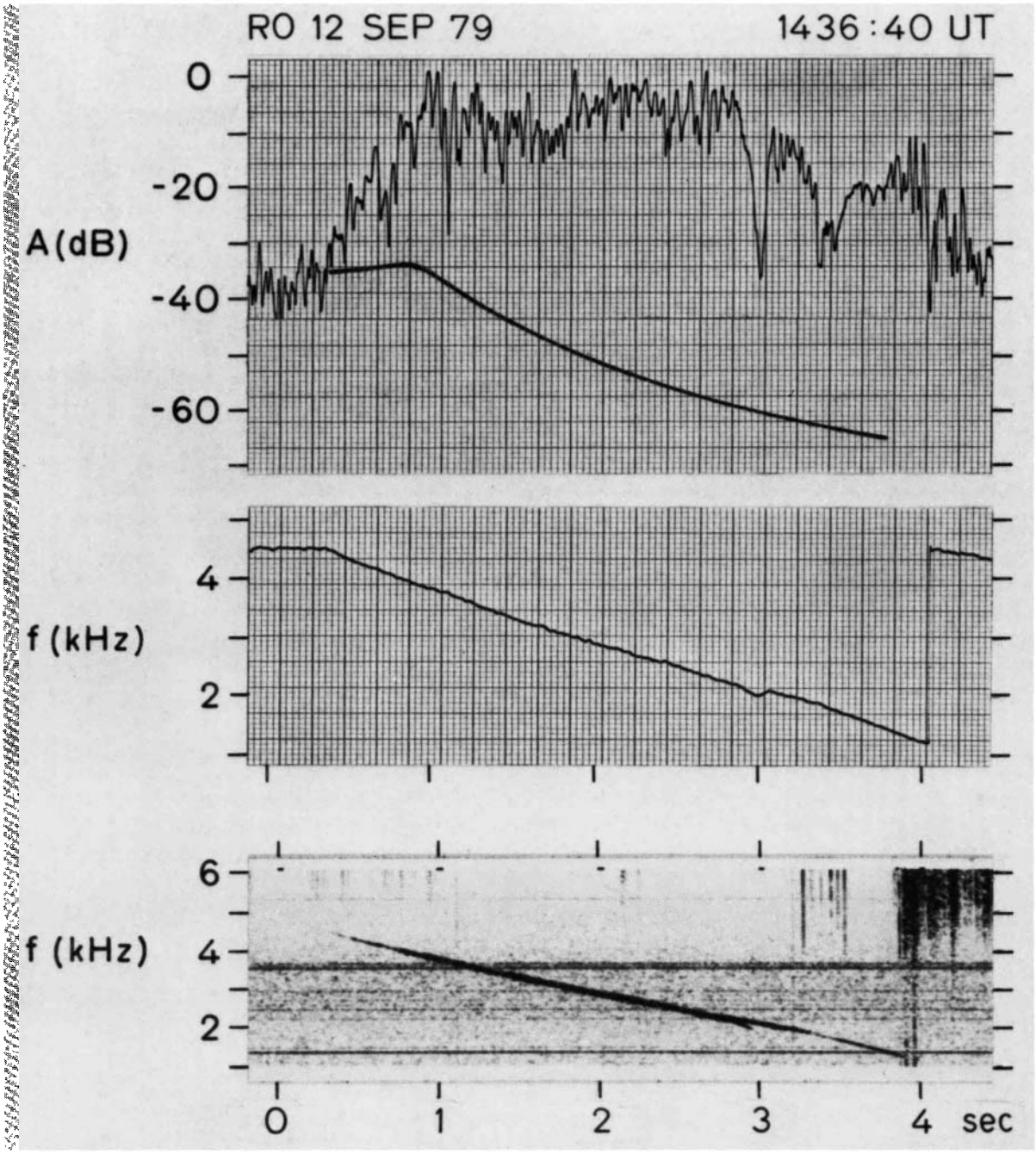

Fig. 13. Details of the −1 kHz/s ramp of Figure 11. Top panel shows amplitude of received signal together with the calculated radiated power profile corrected for ionospheric absorption (smooth curve). Frequency of the tracking filter and the dynamic spectrum are shown in the middle and bottom panels, respectively [*Carlson et al.*, 1985].

cies and amplitudes change with time, that supply energy to the sidebands. They allow carriers of equal amplitude to be relatively unaffected by the triggering process. The result is a pair of unamplified carriers accompanied by prominent sidebands both above and below the carriers.

From the experiments just described we conclude that the magnitude of the modulating signal can be relatively weak and still produce significant sidebands and that these sidebands may grow with time. In this way we can understand how power line radiation, too weak to be detected at its unamplified level, can interact with a carrier from Siple Station to produce sidebands at integer multiples of the difference frequency. Furthermore, the 60-Hz modulation from the power supply of the transmitter might likewise interact with the carrier to produce sidebands that could be amplified independently of the carrier. An example of 60-Hz sidebands is described elsewhere [*Park*, 1981]. In that case the sideband spacing did not change when the carrier was shifted by 10 Hz, which is consistent with the power supply explanation.

An important class of multifrequency interaction is entrainment in which an injected signal from any source captures a self-excited emission by controlling its frequency. An experiment illustrating entrainment is shown in Figure 19

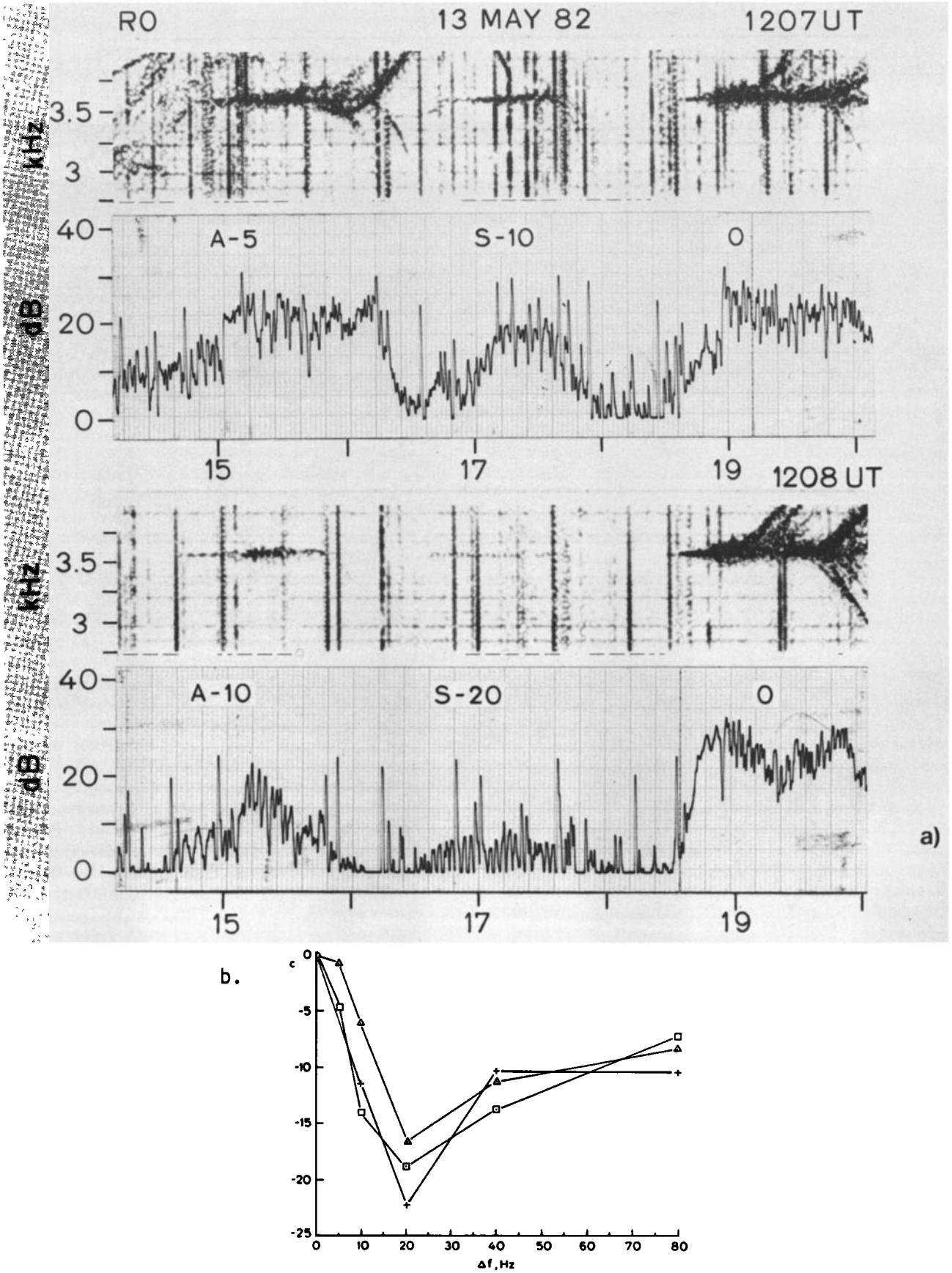

Fig. 14. (a) Response to 1-s pulses with different forms and modulation frequencies (in hertz). A, 100% AM, S, two carriers of equal amplitude. (b) Relative responses to 1-s pulses as a function of modulating frequency. Pluses denote two carriers of equal amplitude; squares, 100% AM; triangles, unity-index frequency modulation [*Helliwell*, 1983*a*].

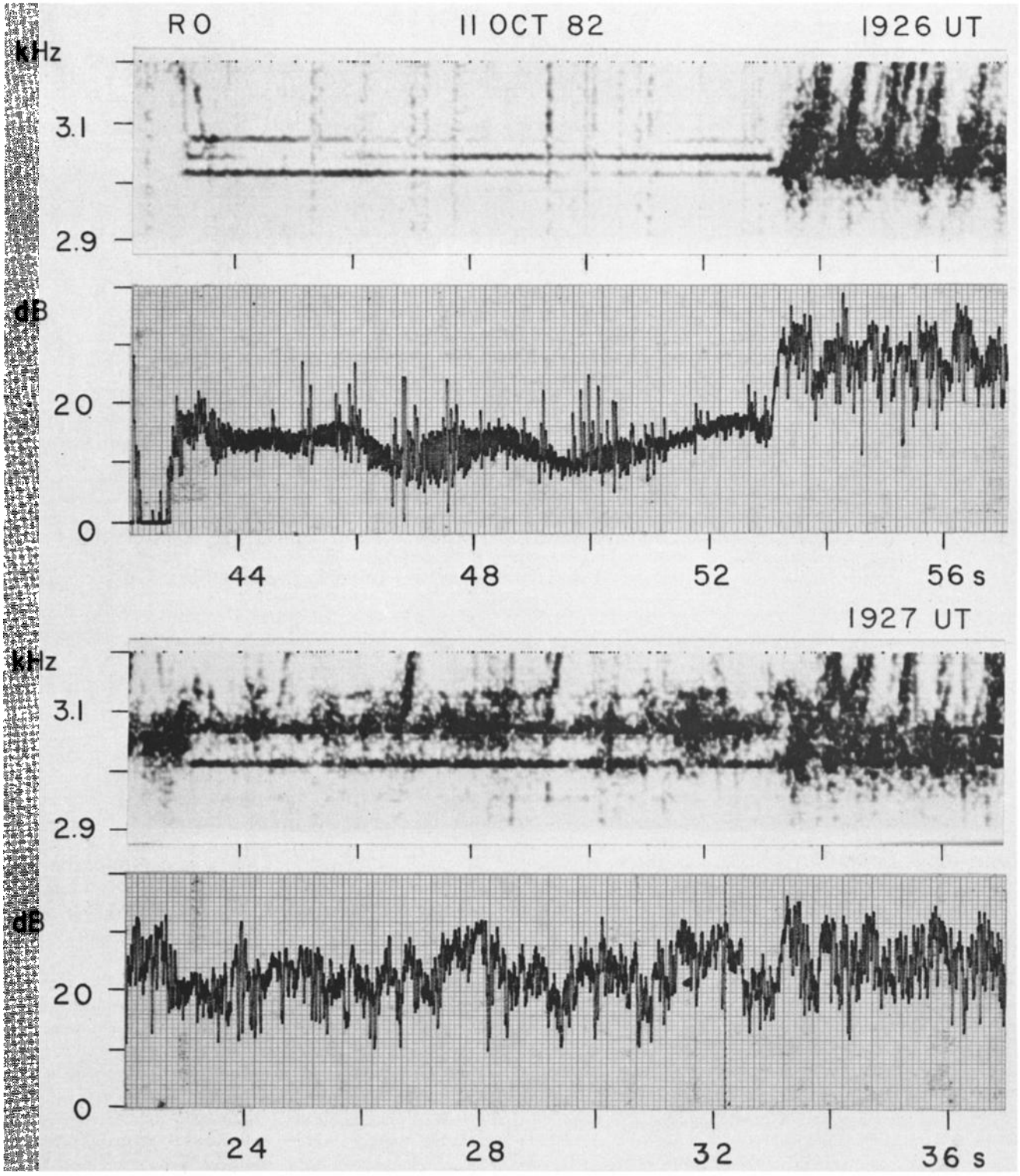

Fig. 15. Line coupling showing transition from two frequencies to one frequency. $\Delta f = 30$ Hz in top two panels; $\Delta f = 60$ Hz in bottom two panels. In each pair of panels the upper panel shows the dynamic spectrum, and the lower panel the rms amplitude [*Helliwell*, 1983*b*].

[*Helliwell*, 1979]. Here the self-excited emission is triggered at the end of a 1-s-long constant frequency pulse. When the frequency of this emission equals the frequency of the rising ramp injected from Siple Station, the rising ramp, which is about 20 dB weaker, entrains the emission until the ramp terminates at its maximum frequency; a falling tone is triggered at the end of the ramp. At the time of encounter there is a weak BLI, a characteristic feature of the entrainment process. The same process is repeated for a ramp of twice the slope, in the right-hand diagram, although the stability of entrainment, as measured by frequency fluctuations, is not as high. On the other hand, it is characteristic of most entrainment events that the entrained signal remains, in an average sense, at or above the frequency of the entrain-

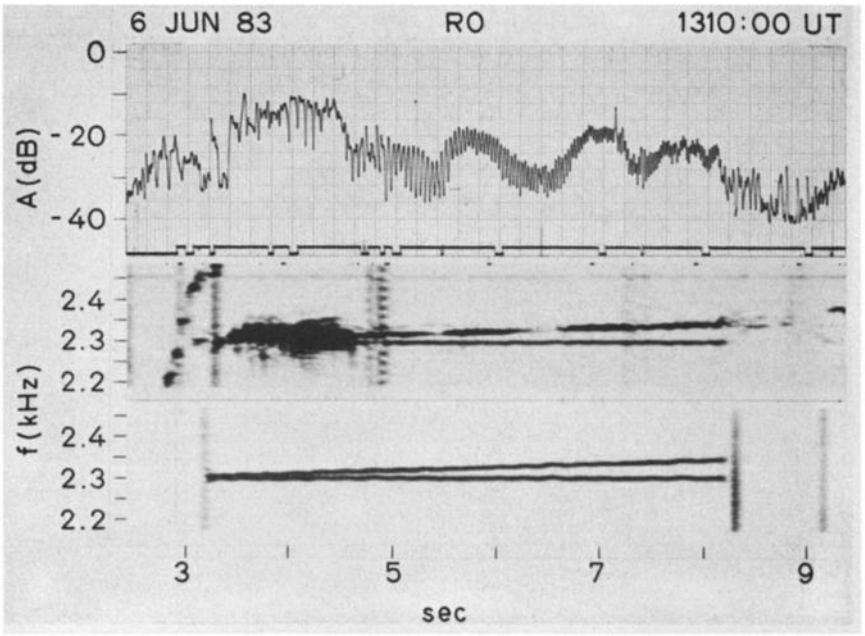

Fig. 16. Equal amplitude beat experiment with Δf varying linearly from 5 to 45 Hz. Spectra of transmitted and received signals are shown in bottom and middle panels, respectively. The sum of the output signals is shown in the top panel [*Helliwell et al.*, 1986*a*].

ing signal. The entrainment experiment provides a possible explanation for the frequent observation of cutoffs and entrainments at the harmonics of power line frequencies seen in natural emissions such as chorus and whistler triggered emissions [*Helliwell and Katsufrakis*, 1974]. An interesting feature of entrainment is the fact that the amplitudes of the free-running oscillation, the entrained oscillation, and the pretriggering amplified signal are all approximately the same. Thus the amplitude of spontaneous free-running oscillations appears to be set not by the triggering signal but by properties of the ambient plasma itself.

A final example of multifrequency interaction, shown in Figure 20, is the spectrum of a six-line signal formed by 100% amplitude modulation of two carriers, one at 2960 Hz and the other at 3320 Hz. This format was designed to simulate power line radiation with 120-Hz spacings. The bottom line triggers a sequence of risers each of which tends to entrain embryo emissions on a succession of lines at higher frequency. These data illustrate the sensitivity of the emission generation process to the presence of nearby signals. We also note that only risers are triggered, never falling tones, while the carriers are present. When this experiment is repeated for $\Delta f = 60$ Hz, growth is less and triggering is largely suppressed, as expected.

A natural extension of discrete multifrequency experiments is the simulation of hiss. Such an experiment is important in the context of the CWI, since the relation of hiss to chorus and other quasi-coherent signals has not been established. Band-limited hiss has been crudely simulated by randomly stepping 10-ms pulses in frequency over a limited band of frequencies. The results of one such experiment are shown in Figure 21. Each second, the same sequence of 100 randomized frequencies is transmitted in a 400-Hz band. Then the bandwidth of the same relative sequence is reduced to ranges of 100, 60, 40, 20, and 0 Hz, with each range being transmitted for 1 s. As can be seen, the intensity increases and the triggering rate increases as the bandwidth approaches 0 Hz. At signal termination we see the characteristic falling tones.

The properties of natural noise at the equator are roughly simulated in this program by virtue of dispersion of the individual 10-ms pulses that travel between the transmitter and the equator. This dispersion causes overlap in group time and randomizes the relative phasing producing amplitude modulation so that the spectrum more closely resembles that of random noise. As shown in Figure 22, the observed received signal from this pseudorandom noise (Figures 22*b* and 22*c*) is comparable in visual appearance on the dynamic display to the noise from a laboratory random noise generator (Figure 22*d*) and a sample of natural magnetospheric hiss (Figure 22*e*). However, in Figure 22*b* we see a repeating pattern (1 s period) of chorus-like elements which are formed from the connection between hiss elements. This new feature of the simulation experiment demonstrates that components of a natural noise spectrum can link together to form a quasi-coherent signal.

From the theory of second-order resonance we deduce that two wavelets separated in frequency and sequential in time will always be in phase with a particular electron at some latitude. This allows two such wavelets to grow collectively, behaving roughly like a frequency ramp that matches the condition for second-order resonance with this electron. The emission created by such a pair of wavelets might then be entrained by the next wavelet and so on until the emission is either cut off by another signal or moves out of the band of growth. That this is a reproducible process is demonstrated by the 1-s repetition shown in Figure 22*b*. On the other hand, only 20 s later the same injected signal shows a different but related pattern. Here the emission grows at the same point in the sequence, but it is much weaker. Such variability suggests that the relative phasing of the wavelets plays a role in getting coherent emissions started. Echoing

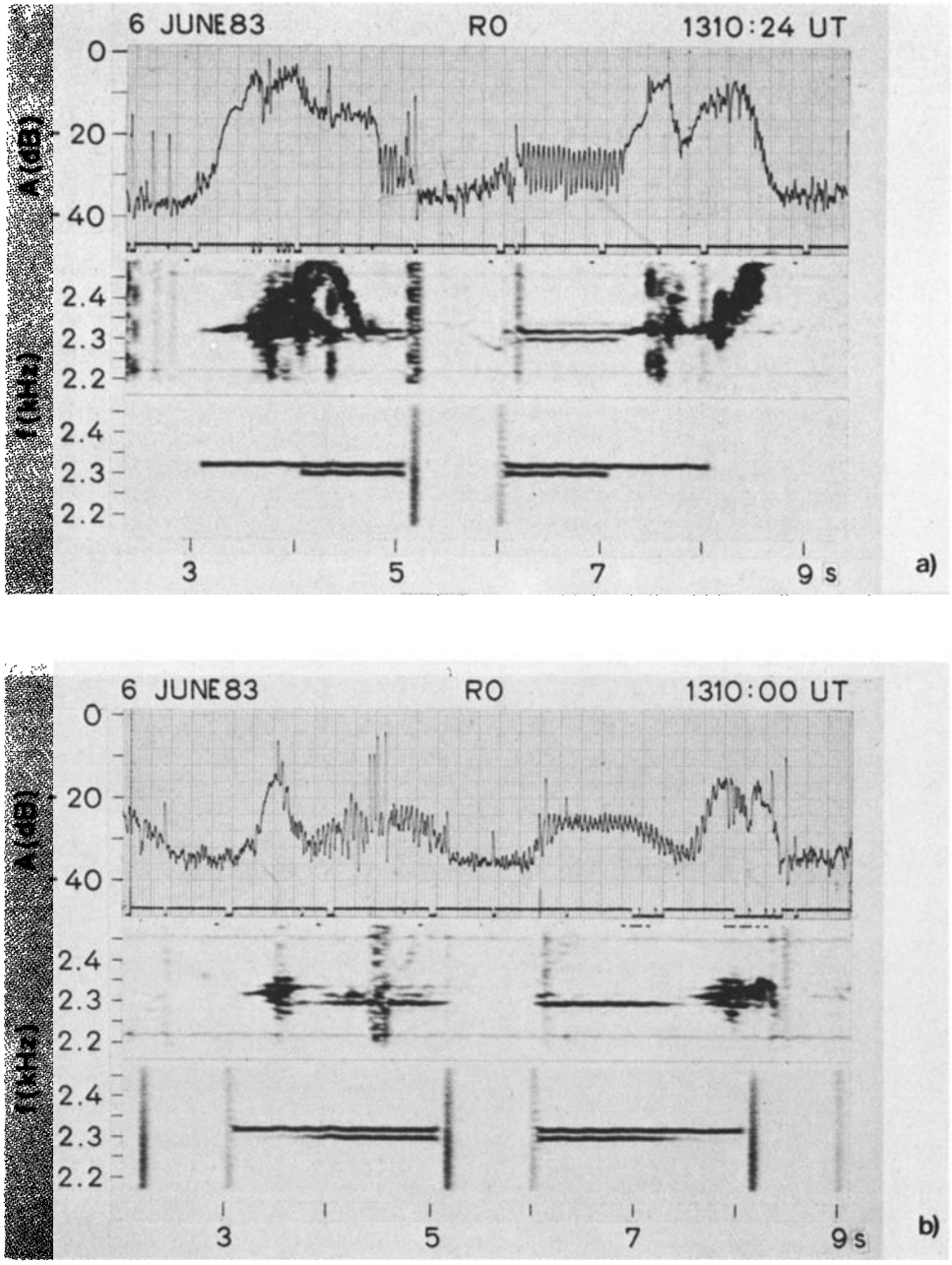

Fig. 17. Beat experiment for $\Delta f = 20$ Hz, showing total amplitude, received spectrum, and transmitted spectrum in top, middle, and bottom panels of each section. (*a*) Lower carrier off in 3–4 s and 7–8 s intervals. (*b*) Lower carrier ramped in amplitude at +20 dB/s and at −20 dB/s in 3–4 s and 7–8 s intervals, respectively [*Helliwell et al.*, 1986*a*].

on the path is also an important factor in maintaining the triggering process. Another factor is the mutual suppression of growth between adjacent wavelets. Suppression may play a role in preventing any single wavelet from reaching saturation when it is embedded in hiss.

The effect of changing the sequence of frequencies is shown in Figure 23, in which the same random sequence is transmitted first in normal form and then in inverted form. In each case the noise band transmitted from Siple is seen to produce little growth within the band itself but many triggered emissions which rise out of the top of the band, a commonly occurring effect in natural hiss bands. In addition, one can see in the background a band of natural hiss whose spectrum does not differ noticeably in appearance from the simulated hiss transmitted from Siple Station. When the pulse sequence is inverted, as in Figure 23*b*, the exact location in time of each triggered riser changes, but the number of emissions per unit time is about the same, indicating that the process is robust in terms of the phasing of the elements. The fact that these emissions can rise well above the noise band can be attributed to the absence of suppressing signals, such as noise, that are close in frequency.

4. Discussion

4.1. *Main Principles and Generalizations*

We now review the principal findings and generalize wherever possible. Reference is made to the specific data from

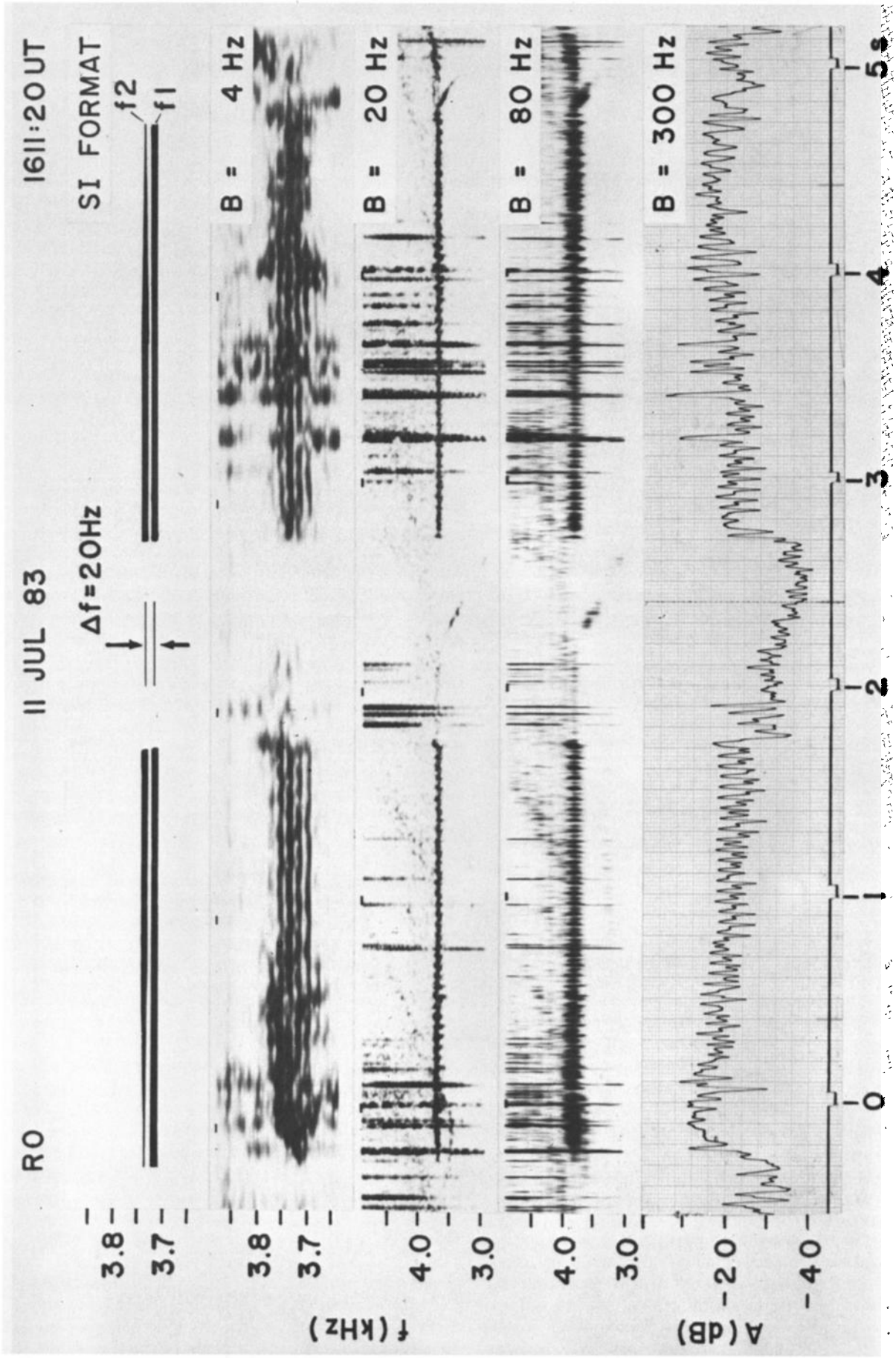

Fig. 18. Beat experiment, similar to Figure 17, except that the amplitude ramp is applied to the upper frequency. To better define the frequency and time domain responses, filter bandwidths of 4, 20, 80, and 300 Hz are used, as shown [*Helliwell et al.*, 1986a].

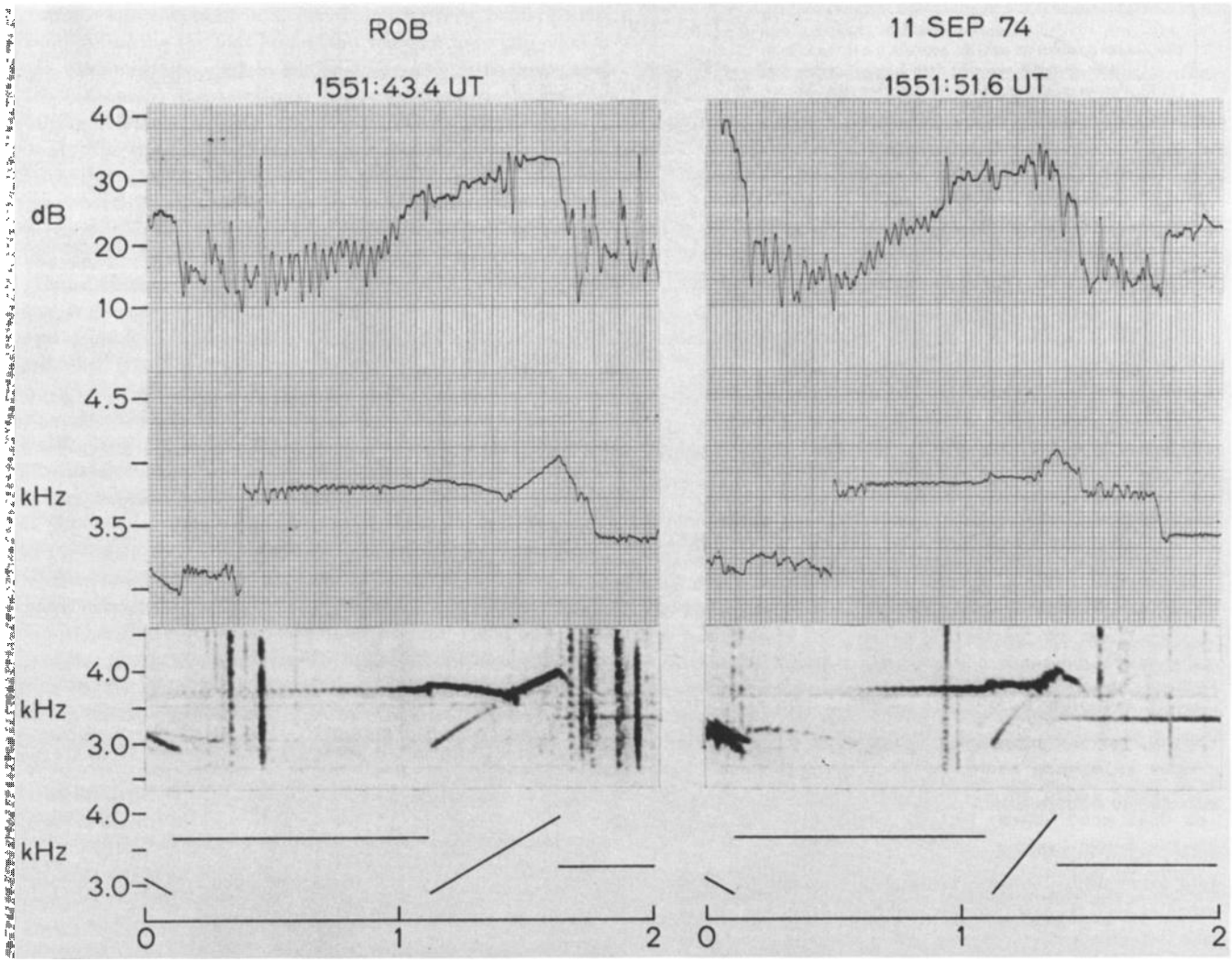

Fig. 19. Two examples of entrainment of triggered emissions by transmitted rising ramps. From top to bottom are shown the tracking filter output, the tracker frequency, the spectrum, and the transmitted format [*Helliwell*, 1979].

which the main principles and generalizations are derived. We consider the following four types of experiments: (1) single-frequency growth and triggering, (2) frequency ramp, (3) multifrequency, and (4) noise simulation. We will endeavor to show that similar basic principles can be applied to both single-frequency and noise signals. We are led therefore to the tentative conclusion that a single mechanism can describe all of the wave generation phenomena observed in the experiments described in this paper.

4.1.1. *Single-frequency growth and triggering.* The step function response of the magnetosphere contains most of the ingredients of a phenomenological description of the coherent wave instability. For step function intensities less than the threshold, B_t, the response is simply the cold plasma transfer function applied to the transmitted pulse. There is no temporal growth or triggering. For input intensities exceeding B_t, exponential temporal growth is usually observed. The saturation value appears to be independent of the intensity of the applied signal. The threshold for the onset of exponential growth is highly variable with time. Often it is close to the maximum power of the transmitter (as in Figure 6), indicating that for some of the time, at least, the instability cannot be triggered with present transmitter powers.

Following saturation there is usually a sequence of risers that continues until the end of the pulse or until echo suppression begins. A riser may begin with a band-limited impulse or simply rise gradually out of the carrier itself. Once the emission has separated from the carrier by 70 Hz or more, the carrier itself will regrow, reach saturation, and trigger another emission, very much like the first. The retriggering time is typically a little less than 1 s (e.g., Figure 20). The resulting emission may reverse its rate of change of frequency and return to the carrier, at which point it will be entrained or cut off. Sometimes there is no triggering of emissions before the end of the pulse. In nearly every case of termination there is an emission at the end of the pulse. There are three forms of this "end" emission. The first is a simple band-limited impulse which covers a range of ~200–500 Hz and may extend both above and below the carrier but primarily above. The second type is self-excited oscillation that starts with a positive frequency offset (PFO) and

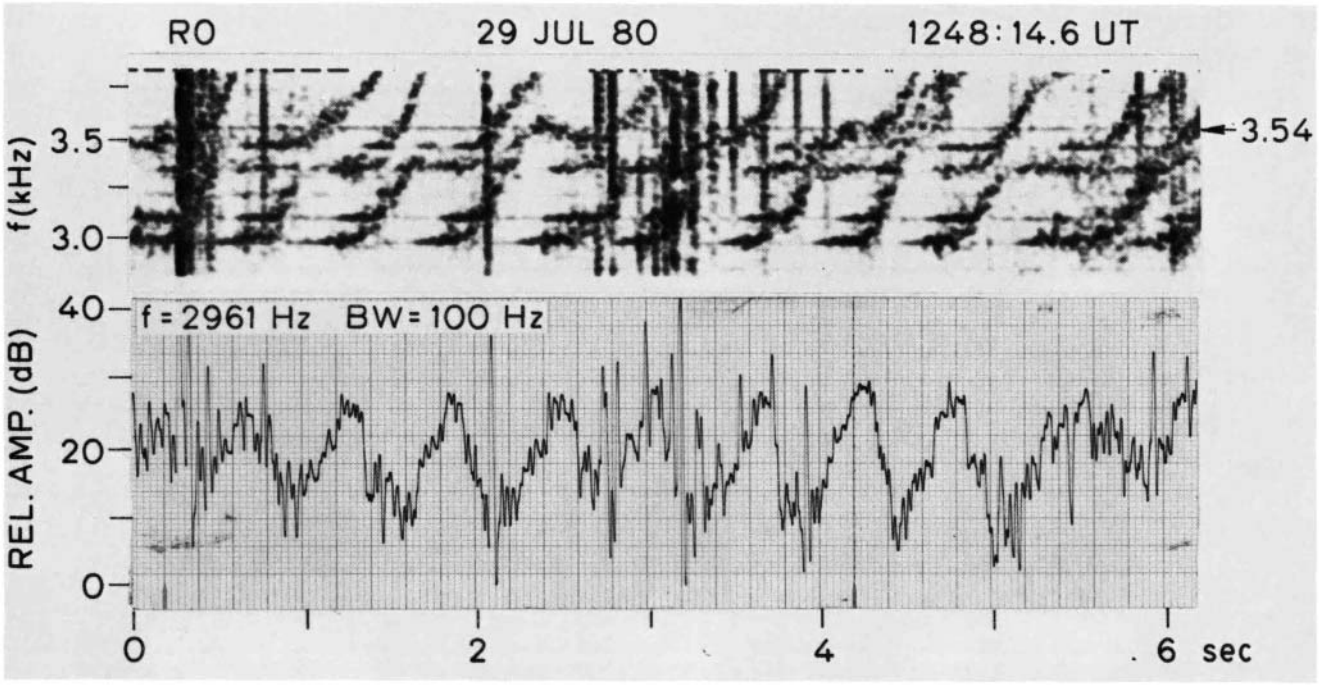

Fig. 20. Six-line spectrum formed by 100% amplitude modulation of two carriers at $f_1 = 2960$ Hz and $f_2 = 3320$ Hz [*Helliwell*, 1983*b*].

usually continues with a decreasing frequency. The third case of termination or end triggering is a combination of the BLI and the PFO.

It is interesting to note by comparing Figures 6 and 19 that the pretermination triggering events sometimes look very much like the termination events, showing both a BLI and a positive frequency offset. The only difference is that in the pretermination case the emission usually rises with time. However, there are cases where pretermination triggering occurs and the emission rapidly falls and is reabsorbed by the carrier. This process probably accounts for much of the spectrum spreading that appears mainly on the upper side of the carrier. Likewise there are cases of termination triggering in which the PFO is followed by a rising emission, as in Figure 8. An important feature of triggered emissions is that a CW wave does not trigger falling tones before its termination.

Virtually all cases of temporal growth are accompanied by phase advance of the output signal, as in Figure 6. The phase function is usually parabolic, corresponding to a linear increase in frequency with time. Such behavior can be explained in terms of second-order resonance at a location slightly downstream from the magnetic equator. At the time of triggering the rate of change of phase suddenly increases, as shown in Figure 6*c* at 2.0 s. A triggered riser often exhibits a distinctive increase in bandwidth (of the riser) which is evidenced by strong amplitude and frequency modulation, as illustrated in Figure 6*a*. The triggered riser, being a self-excited oscillation, is more subject to control by the ambient noise components at the input to the interaction region, thus accounting for the observed spread in the riser's spectrum.

It should be emphasized that these features of triggering are related to single-frequency input signals. Multifrequency signals produce different kinds of results.

4.1.2. *Frequency ramps.* Closely related to the CW signals described above is the frequency ramp. This is a signal whose frequency changes slowly with time (about a few kilohertz per second). Virtually the same rules for onset of growth, growth itself, and saturation apply to ramps as to CW signals. Thus all triggering by frequency ramps begins above the ramp frequency even though the absolute df/dt may be negative. At the end of a ramp a PFO usually occurs, and the resulting emission may be either a faller or a riser. An additional feature of interest is the relation between the asymptotic slope of a triggered riser and the slope of the ramp itself. Thus if the magnitude of the asymptotic slope of the riser (or faller) is 1 kHz/s and if the slope of the applied frequency ramp is also of the same magnitude, there is usually no triggered emission, only growth. When a rising ramp terminates, then the triggered riser is a simple extension of the ramp with only slight changes in slope. On the other hand, if the ramp slope is reversed, the termination emission may turn into a hook consisting of an initial falling portion followed by a riser that reaches the same asymptotic slope of 1 kHz/s. Examples of both types of emissions from falling and rising ramps are shown in Figure 11.

Frequency ramps show variability in triggering, a feature not seen in monochromatic signals. This results from the fact that the growth rate can vary with time as a result of the change of growth rate with frequency. Thus in the case of Figure 11 the initial parts of the slower (less than −1 kHz/s slope) falling ramps trigger sequences of risers. Below a frequency of ~3 kHz the triggering ceases, possibly as a result of the input signal having dropped below the threshold for growth. Furthermore, triggering ceases when the absolute slope exceeds a critical value. As a result, phase-locked growth may extend to a lower than normal frequency.

The −1 kHz/s ramp in Figure 13 is a good demonstration of this idea. Because the maximum slope of the triggered emissions is comparable with the slope of the injected sig-

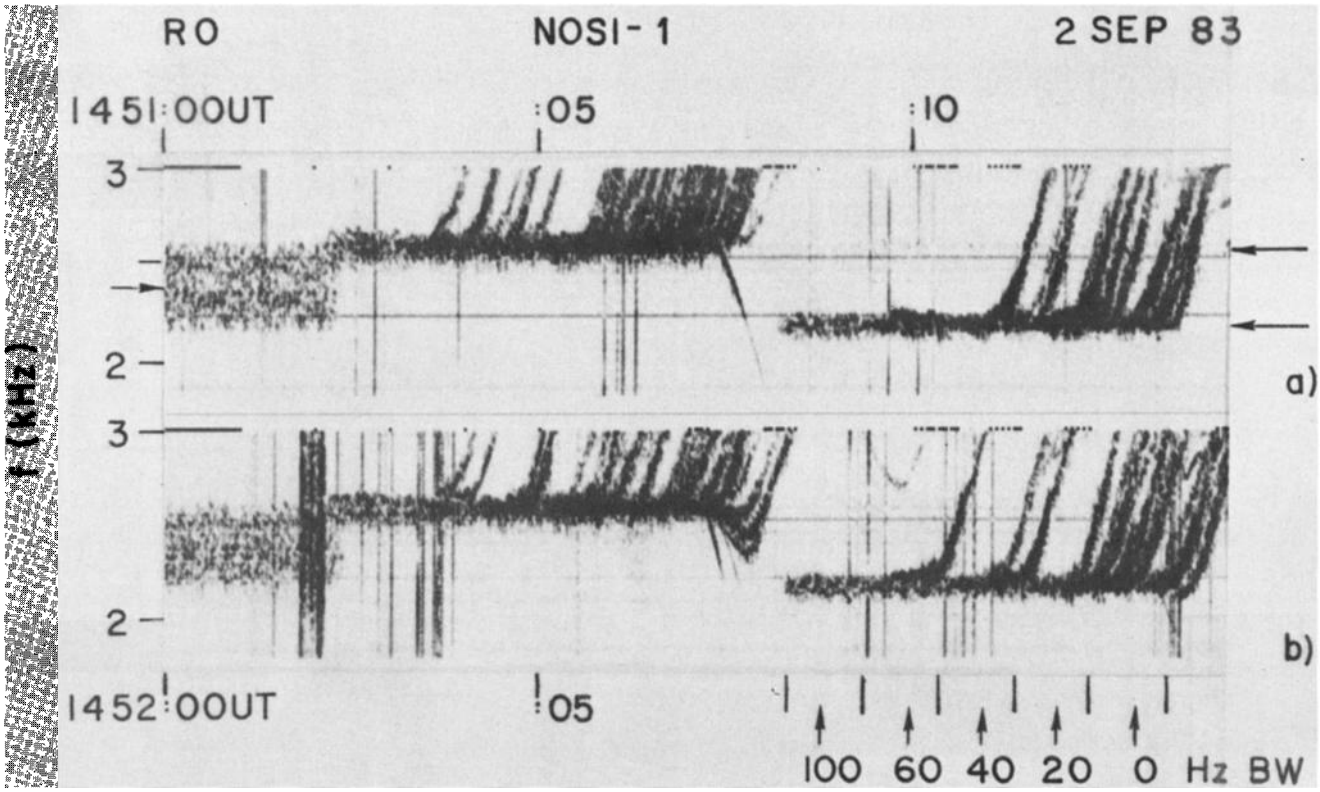

Fig. 21. Two samples of a 400-Hz band of simulated hiss, each followed by two sequences of five contiguous 1-s pulses of hiss with 100, 60, 40, 20, and 0 Hz bandwidth. The average intensity increases about 10 dB as the bandwidth is reduced to zero. Arrows mark centers of hiss bands [*Helliwell et al.*, 1986*b*].

nal, there is no triggering over most of the ramp. The result is that the frequency of the fully amplified signal falls to a much lower value than is the case for other ramps that show triggering. One way to explain this effect is to argue that the loop gain is just sufficient to sustain a saturated signal at the lower frequencies but is not sufficient to start the growth process in the presence of ambient noise. The main point is that phase-locked growth produces an output signal that is well above the background noise which we assume limits the threshold for growth. As a result the background noise cannot interfere with the phase-bunching process over most of the interaction region because of the strong spatial growth. However, the same input signal applied in the absence of spatial growth would have to contend initially with ambient noise over the entire interaction region, thus preventing growth from starting. Hence the ramp is able to move into the frequency range where the unamplified input signal has fallen below the ambient noise level. Using the antenna response pattern of Figure 4 and the observed intensity of the unamplified signal and the saturation levels of Figure 13, we deduce that the maximum ratio of the saturation level to the threshold is 55 dB. This means that the signal level at which spatial growth can be controlled is much lower than that at which temporal growth begins. As the ramp slope is increased in magnitude, the growth tends to decrease or disappear altogether. As noted in connection with the description of the data, this effect can be attributed to a reduction in the flux of electrons associated with the increase in parallel resonant velocity as the region of second-order reasonance moves away from the magnetic equator.

4.1.3. *Multifrequency interactions.* When two or more frequencies are present simultaneously in the magnetosphere, several very interesting effects occur. The first is entrainment, illustrated in Figure 19, where a free-running oscillation is captured by an injected signal. Such a signal may be a weak radiation component from a ground-based power grid or a ground-based transmitter. As the example shows, the required intensity of the entraining signal is low, in this case 20 dB below saturation. The mechanism of entrainment, which seems to be related to cutoff, is not known. Entrainment occurs so rapidly for the case in which fallers are entrained by injected risers that there is inadequate time available for the interaction region to drift to the location of second-order resonance for the entraining signal. Thus it appears that entrainment actually takes place at the location of the free-running oscillation even though the df/dt after entrainment is not correct for second-order resonance at that location. In order for this to happen it is necessary for the wave itself to control the phasing of the phase-bunched currents. This may require that the amplitude of the output signal of the entrained emission be high enough to trap a significant fraction of the resonant particles. Such trapping might then take the place of the inhomogeneity in determining the phasing of the electrons with respect to the wave. This mechanism puts a limit on the minimum value of the output signal. It has been estimated in conjunction with wave-induced particle precipitation events that the discrete emissions have peak amplitudes of ~5 pT [*Chang and Inan*, 1985]. The trapping limit for signals near half the gyrofrequency at $L = 4$ inside the plasmapause is 1–2 pT. Thus the adopted values for intensity are consistent with trapping of

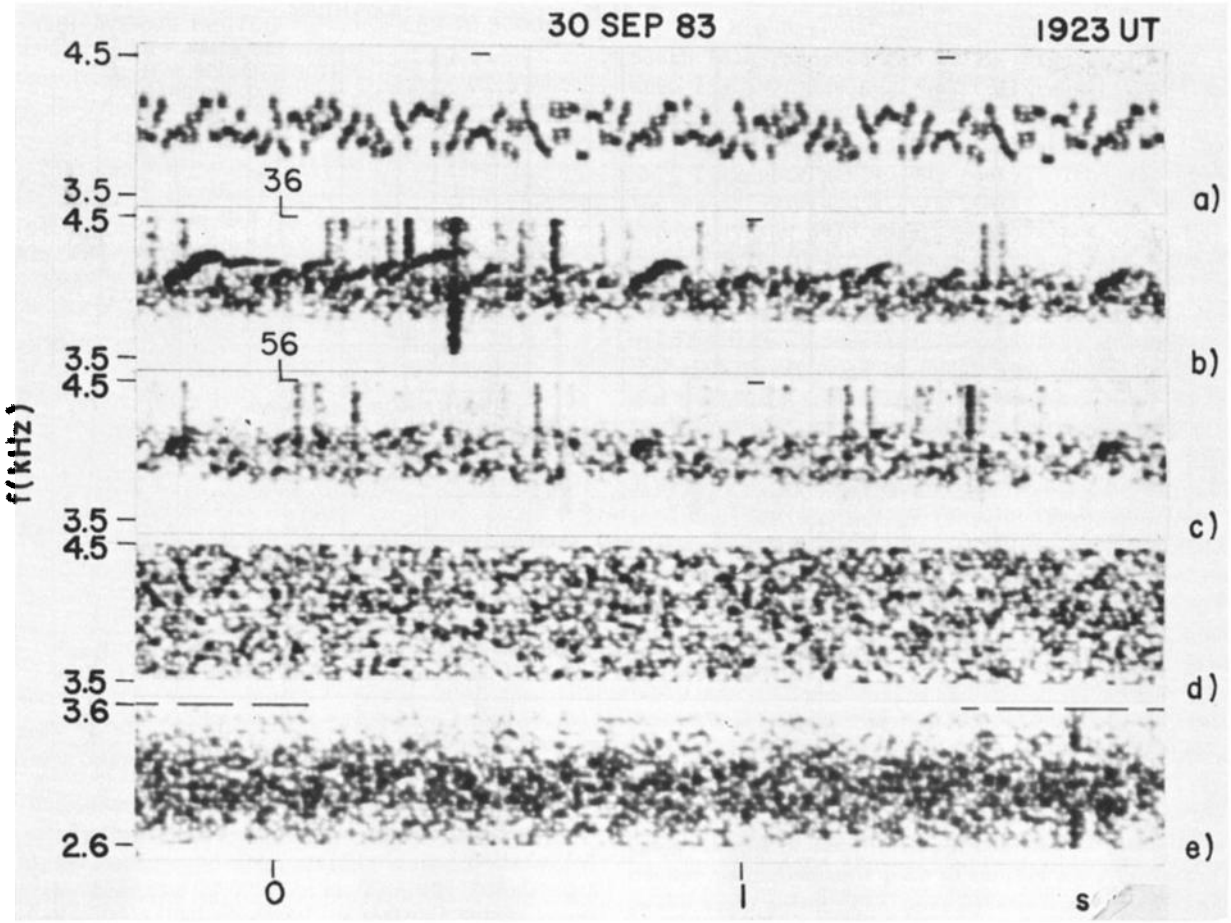

Fig. 22. Hiss spectra for 20 Hz filter bandwidth. (*a*) Transmitted spectrum, with 1-s periodicity. (*b*) and (*c*) Two segments of spectra, taken 20 s apart, of the pattern in Figure 22*a*, as received at Roberval. (*d*) Spectrum of hiss from a laboratory random noise generator. (*e*) Spectrum of natural hiss recorded at Roberval on February 14, 1977, 1216 UT [*Helliwell et al.*, 1986*b*].

electrons at saturation. This problem merits further study.

Closely related to entrainment in terms of the separation of frequency components is the suppression of growth. Here we deal generally with two injected signals, each growing at different frequencies. When the spacing between the signals is 20 or 30 Hz, each signal suppresses the growth of the other almost completely. As Δf is increased above 30 Hz, the upper component grows more than the lower; when Δf reaches 100 to 200 Hz, the two signals grow independently at their single-frequency rates. Asymmetry in the suppression properties between two such signals is generally seen in all two-frequency experiments. Since recovery from suppression as demonstrated by Figure 15 is virtually instantaneous, it is suggested that the suppression process involves waves interacting with waves rather than the delayed interaction envisioned in the quiet band effect [*Raghuram et al.*, 1977; *Cornilleau-Wehrlin and Gendrin*, 1979; *Matthews et al.*, 1984]. In the delayed model, waves in the output region disturb the distribution of particles, which then travel back to the equator where, as a result of their altered distribution, they cause less growth of the lower-frequency signals with which they resonate. We look therefore for some inherent asymmetry in the interaction process. This can be found readily in the case of second-order resonance, where electrons with parallel velocities less than the equatorial resonance value are nowhere resonant with the wave, while electrons with velocities higher than the equatorial resonance value will experience first-order resonance at two points symmetrically situated on either side of the equator [*Helliwell*, 1970]. However, no analysis along these lines has yet been carried out.

Closely connected with suppression is the generation of sidebands. The conditions are about the same, with sidebands being created whenever there is appreciable interaction between adjacent signals. Examples are shown in Figures 15, 17, and 18. Sometimes as many as seven orders of sidebands can be seen spaced about the two carriers by the separation frequency, as shown in Figure 16. As mentioned in section 3, an explanation for such sideband generation can be found using time domain data on temporal growth. Thus each beat is treated as an independent coherent signal whose time duration is the reciprocal of the frequency difference. This signal begins to grow during the beat, and when the beat approaches its null, the emission rises in frequency just as in the case of termination triggering. The following beat tends to suppress growth of that particular emission. The process then repeats on the next beat, and very quickly a uniform series of interbeat emissions is created, as shown in Figure 19. These emissions are fundamentally the same as those described in Figure 1, except for their duration. They will tend to grow exponentially with time and the phase will tend to advance. Furthermore, the

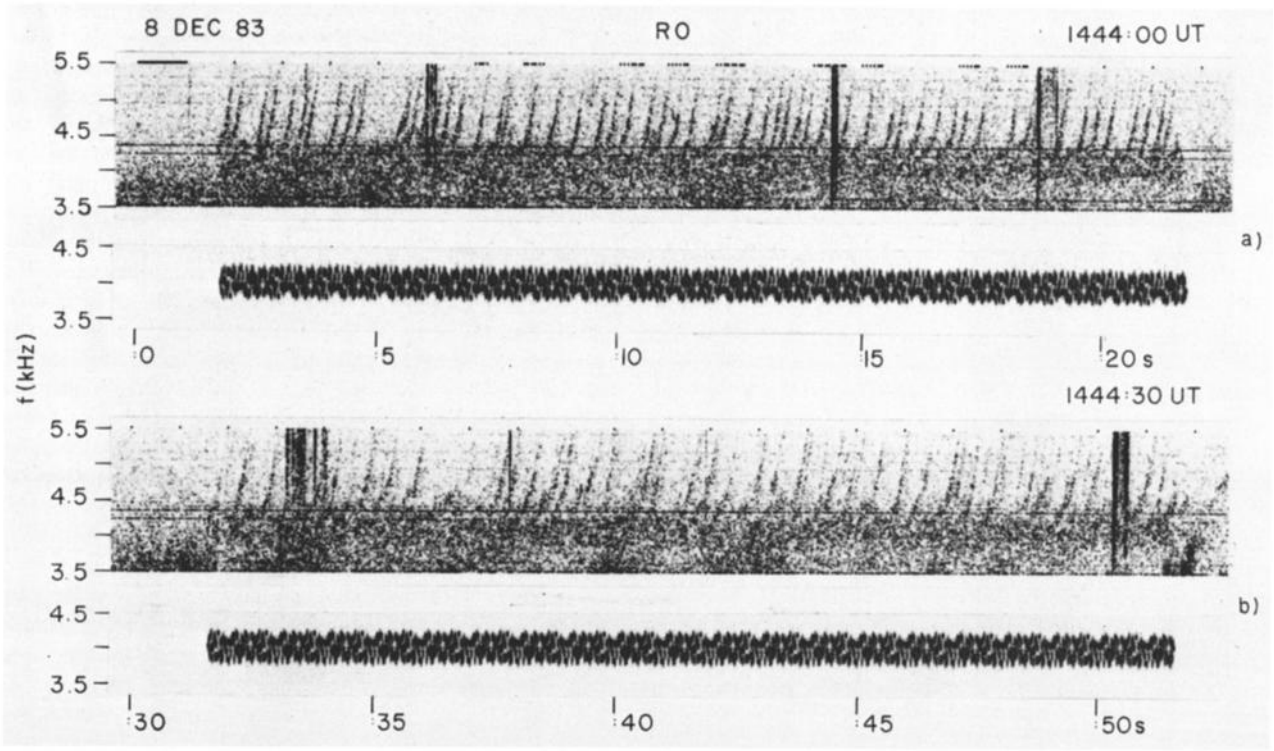

Fig. 23. (*a*) Four-hundred-hertz hiss band triggering chorus with 1-s periodicity. (*b*) Same as in Figure 23*a* but with inverted sequence of element frequencies [*Helliwell et al.*, 1986*b*].

discontinuity represented by the null in the beat will produce further frequency changes of the same type seen in the positive frequency offset. The result is a significant amount of frequency modulation as well as amplitude modulation. The phasing between these two modulation cycles will determine the relative amount of energy in the upper and lower sidebands, as can be readily demonstrated from modulation theory.

An interesting and exciting feature of the sideband experiments is the presence of subharmonics. Their frequencies appear to follow repeatable patterns related to integer val ues of subharmonics [*Sa and Helliwell*, 1988]. Included in the subharmonic category are sidebands whose amplitudes exceed the amplitude of the weaker member of the input pair. It is possible to generate significant subharmonic components when one of the two carriers is 40 dB below the other. In addition, the amplitude of that weak sideband signal may grow to a value comparable with the stronger signal itself. It appears that in general as long as a coherent wave is present near the frequency of an injected signal, say within 100 Hz, there is likely to be a significant interaction, with a resulting sideband structure that depends directly on the frequency difference between the two carriers and on the ratio of their amplitudes. This finding from the Siple Station experiments provides a ready explanation for the somewhat puzzling data on power line radiation in the magnetosphere. Although there is clear evidence for growth and interaction at harmonics of the power system, it has been difficult to measure directly the unamplified signal from the power grids. These new experiments from Siple show that significant interaction can occur when the intensity of a power line harmonic is more than 40 dB below that of the Siple signal. Since many satellite detectors cannot detect such weak signals, it can be understood why they have not been better documented up to this time.

4.1.4. *Noise simulation.* The breakup of coherent signals through the sideband mechanism has its "inverse" in the noise simulation experiments. Here, as shown in Figure 22, small wavelets representing the components of random noise may link together in the magnetosphere to form longer quasi-coherent wave trains. When these extended wave trains become long enough, they resemble chorus elements. It is readily understood from the theory of second-order resonance that any two wavelets can be linked together by cyclotron resonant electrons at a particular latitude that depends on the frequency and phase differences between the two wavelets. This feature of interaction coupled with entrainment provides a basis for explaining the creation of an extended coherent wave train.

In the case of strong echoing between two conjugate points the various wavelets will change their relative phases as well as their group times, and hence the conditions for coherent growth will continually change. With the growth of chorus-like elements there is an increase in the generation of sidebands resulting from the beating between chorus elements that overlap in time. Thus there is simultaneous generation of sidebands by some elements in the dynamic spectrum and the coalescence of other elements into more extended coherent wave trains. Such an equilibrium could explain the combination of hiss and chorus that is characteristic of natural noisebands under conditions of good echoing.

However, chorus embedded in hiss is also seen outside the plasmasphere where echoing is very weak. In this case it is necessary to adopt some additional mechanism. One

possibility is that the background thermal noise is able to create wave packets on the downstream side of the equator that will grow to a certain amplitude and duration after which they are limited by the suppressing effect of adjacent wave packets that have started to grow in the same vicinity. Under favorable conditions some of these wavelets will grow to full saturation levels and hence become strong chorus elements. The result is a statistical distribution of wavelets that when observed on a satellite looks like a superposition of hiss and chorus.

Putting noise simulation experiments together with suppression experiments leads to another new experiment in which simulated noise is used to suppress growth of a coherent wave. The addition of simulated noise to a coherent signal reduces the growth of the latter. From this result we deduce that the coherent wave signal itself might be used to indirectly measure the "invisible" background noise that populates the magnetosphere but cannot be seen on the ground. This is noise that is nonducted, such as plasmaspheric hiss, and hence is unable to cross the lower boundary of the ionosphere and be detected on ground-based receivers. However, the same noise is expected to pass through any duct in the magnetosphere and hence create a noise background that could suppress the growth of ducted waves. By transmitting simulated noise for calibration one could obtain the effective value of the hidden noise in the magnetosphere. Thus it may be possible to use this proposed ground-based technique to map the distribution of nonducted noise thought to be responsible for much of the precipitation of particles from the radiation belts.

4.2. *Comparison With Theories*

As mentioned earlier there are no complete theories of the phenomena reviewed in this paper. It is not the intention here to review this particular subject. Readers are referred to the Ph.D. thesis by *Carlson* [1987] for an up-to-date review of theoretical work on the CWI. Included in that thesis are the results of a test particle model of the CWI, giving predictions of the phase advance, growth, and saturation shown in Figure 6. The main limitation of this model is that the electron distribution function must be limited to a relatively small parallel velocity range (<1%) in order to control the numerical errors associated with large numbers of test particles. On the other hand, a case can be made that the chosen distribution function is indeed representative of what actually happens. It is clear at this point that broader parallel velocity distributions must be tried in order to establish the adequacy of the model. Furthermore, the model needs to be extended to the case of two or more frequencies in order to explain sidebands and the various transient phenomena (e.g., BLI and PFO) that have been observed.

5. FUTURE DIRECTIONS

In this section we discuss the possibilities for new controlled VLF wave injection experiments in the Earth's magnetospheric plasma. As has been demonstrated, such experiments can provide quantitative information on the properties of the CWI, a basic process of natural plasmas. We have noted the uniqueness of the Siple Station facility as it presently exists for the performance of such experiments. It is recognized that a space-borne transmitter would complement these ground-based experiments by providing access to a full range of wave normals and possibly larger in situ field intensities. On the other hand, space experiments cannot replace those performed on the ground, since a fixed location is necessary to separate space and time variations. It is more likely that the two kinds of experiments will complement one another in an overall study of the mechanisms and effects of the coherent wave instability.

In the near future, it is unlikely that a more economical means for systematic experimentation on the CWI can be found than an Antarctic-based transmitter facility. Accordingly, attention should be given to an extension of the present Antarctic experiments. Although Siple Station has been a quite satisfactory location scientifically, other locations on the West Antarctic ice sheet may provide advantages either scientifically or logistically and hence should be thoroughly evaluated. Once a location is selected, the characteristics of a new wave injection facility can be defined: Clearly, more effective radiated power is needed. How this might best be achieved is an open question. Higher-power transmitting equipment could be used with a single crossed dipole array, but the cost of such equipment rises rapidly with power. Another solution is to employ an array of phased antenna elements with lower-power transmitters driving each one. Such an array could provide beaming, which would have the advantage of not only increasing the effective radiated power at a particular entrance point into the ionosphere but could provide information on the location of ducts. The use of a polarized antenna has been demonstrated to provide a significant increase in effective radiated power. Employing these ideas, one could imagine an array of crossed dipoles, such as that shown in Figure 1*c*, in which four sets of crossed dipoles are arranged in a broadside array and phased so as to maximize the wave intensity at a particular point of injection at the lower boundary of the ionosphere. Simple power amplifiers might be arranged to drive each antenna with linkages to a master control which would provide the required modulation and phasing. Control of corona is an important problem and may require the use of high-voltage hardware.

On the operational side, new experiments would benefit from having the signal spectrum as received at the conjugate point made available in real time to the transmitter operator. Consideration should be given to the use of a real-time satellite link capable of handling a bandwidth of 10 kHz and a dynamic range of 50 dB. Such a link would relay the signal from the conjugate point back to the transmitter, where it would be displayed on a real-time spectrum analyzer. Then the conditions of the experiment could be altered in virtually real time, with a delay of no more than a few seconds, in order to optimize the parameters and to discover for example the polarization that would produce the best null on a particular path. Such a facility would make it much easier to take advantage of short-term phenomena that require operator control.

Finally, we note that coherent wave injection can be used to study wave-induced electron precipitation. The SEEP satellite experiments showed that pulses from a VLF transmitter can precipitate detectable fluxes of electrons [*Imhof et al.*, 1983]. These experiments have opened up an entirely new area of investigation of the properties of natural plasmas. We also know that lightning-induced whistlers generate detectable bursts of X rays, ionization, and light, all

of which are attributed to VLF wave-induced electron precipitation. Since the saturation levels reached by Siple excited emissions are the same as those produced by whistlers, it is clear that the Siple signals are capable of producing similar effects. What is needed is sufficient power to reach the threshold for growth on paths with low enough equatorial electron concentration (outside plasmapause) and at low enough wave frequencies to scatter >40-keV electrons. Siple Station has exceeded the threshold power for growth and emission triggering in the low-density ($\sim$10 el/cm^3) equatorial region just outside the plasmapause (D.L. Carpenter, private communication, 1988). This is close to the 10–20 el/cm^3 concentration characteristic of the January 2, 1971 event in which natural whistlers excited X rays as a result of triggered emissions outside the plasmapause [*Rosenberg et al.*, 1971]. Thus the input wave intensity required for the precipitation of >30-keV electrons appears to have been reached with the new 42 km cross. More frequent access to the low-density region outside the plasmapause can be expected to result from the use of more power. One way to increase the effective radiated power is to employ a directive antenna array that concentrates the available power in the desired direction. Such an upgraded facility would provide new insights into one of the most fundamental and interesting phenomena observed in plasmas of all kinds. Such knowledge is necessary to a full understanding of the Earth's magnetosphere, laboratory plasmas, and astrophysical plasmas. Furthermore, use of such facilities for regular plasma diagnostic measurements from the ground are an exciting and as yet untapped resource.

Acknowledgments. This work was supported under National Science Foundation Division of Polar Programs grant DPP-8613783. The typescript was prepared by G. Walker.

REFERENCES

Bell, T. F., U. S. Inan, and R. A. Helliwell, Nonducted coherent VLF waves and associated triggered emissions observed on the ISEE 1 satellite, *J. Geophys. Res., 86,* 4649, 1981.

Bell, T. F., U. S. Inan, I. Kimura, H. Matsumoto, T. Mukai, and K. Hashimoto, EXOS-B/Siple VLF wave-particle interaction experiments, 2, Transmitter signals and associated emissions, *J. Geophys. Res., 88*, 295, 1983*a*.

Bell, T. F., H. G. James, U. S. Inan, and J. P. Katsufrakis, The apparent spectral broadening of VLF transmitter signals during transionospheric propagation, *J. Geophys. Res., 88,* 4813, 1983*b*.

Bell, T. F., J. P. Katsufrakis, and H. G. James, A new type of VLF emission triggered at low altitude in the subauroral region by Siple Station VLF transmitter signals, *J. Geophys. Res., 90*, 183, 1985.

Bernhardt, P. A., Theory and analysis of the 'super whistler,' *J. Geophys. Res., 84*, 5131, 1979.

Carlson, C.R., Simulation and modeling of whistler mode wave growth through cyclotron resonance with energetic electrons in the magnetosphere, Ph.D. thesis, Stanford University, Stanford, Calif., June 1987.

Carlson, C. R., R. A. Helliwell, and D. L. Carpenter, Variable frequency VLF signals in the magnetosphere: Associated phenomena and plasma diagnostics, *J. Geophys. Res., 90*, 1507, 1985.

Carpenter, D.L., and Z.T. Bao, Occurrence properties of ducted whistler mode signals from the new VLF transmitter at Siple Station, Antarctica, *J. Geophys. Res., 88*, 7051, 1983.

Carpenter, D. L., and C. G. Park, On what ionospheric workers should know about the plasmapause-plasmasphere, *Rev. Geophys., 11*, 133, 1973.

Carpenter, D.L., A. J. Smith, and T.F. Bell, The Siple VLF transmitter as a multi-frequency probe of the earth-ionosphere waveguide, *J. Atmos. Terr. Phys., 50*, 105, 1988.

Chang, D.C.D., and R.A. Helliwell, Emission triggering in the magnetosphere by controlled interruption of coherent VLF signals, *J. Geophys. Res., 84*, 7170, 1979.

Chang, D. C. D., and R. A. Helliwell, VLF pulse propagation in the magnetosphere, *IEEE Trans. Antennas Propag., AP-28*, 170, 1980.

Chang, H. C., and U. S. Inan, Test particle modeling of wave-induced energetic electron precipitation, *J. Geophys. Res., 90*, 6409, 1985.

Cornilleau-Wehrlin, N., and R. Gendrin, VLF transmitter-induced quiet bands: A quantitative interpretation, *J. Geophys. Res., 84*, 882, 1979.

Dowden, R. L., A. C. McKey, L. E. S. Amon, H. C. Koons, and M. H. Dazey, Linear and nonlinear amplification in the magnetosphere during a 6.6-kHz transmission, *J. Geophys. Res., 83*, 169, 1978.

Gurnett, D.A., and U.S. Inan, Plasma wave observations with the Dynamics Explorer 1 spacecraft, *Rev. Geophys.*, in press, 1988.

Helliwell, R. A., *Whistlers and Related Ionospheric Phenomena*, Stanford University Press, Stanford, California, 1965.

Helliwell, R. A., A theory of discrete VLF emissions from the magnetosphere, *J. Geophys. Res., 72*, 4773, 1967.

Helliwell, R.A., Intensity of discrete VLF emissions, in *Particles and Fields in the Magnetosphere*, edited by B.M. McCormac, p. 292, D. Reidel Publishing Co., Dordrecht, Holland, 1970.

Helliwell, R. A., Siple Station experiments on wave-particle interactions in the magnetosphere, in *Wave Instabilities in Space Plasmas*, edited by P. J. Palmadesso and K. Papadopoulos, p. 191, D. Reidel Publishing Co., Dordrecht, Holland, 1979.

Helliwell, R. A., Controlled stimulation of VLF emissions from Siple Station, Antarctica, *Radio Sci., 18*, 801, 1983*a*.

Helliwell, R.A., VLF wave injections from the ground, in *Active Experiments in Space, Spec. Publ., SP-195*, p. 3, 1983*b*.

Helliwell, R. A., and U. S. Inan, VLF wave growth and discrete emission triggering in the magnetosphere: A feedback model, *J. Geophys. Res., 87*, 3537, 1982.

Helliwell, R. A., and J. P. Katsufrakis, VLF wave injection into the magnetosphere from Siple Station, Antarctica, *J. Geophys. Res., 79*, 2511, 1974.

Helliwell, R. A., and J. P. Katsufrakis, Controlled wave-particle interaction experiments, in *Upper Atmosphere Research in Antarctica, Antarct. Res. Ser.*, Vol. 29, edited by L. J. Lanzerotti and C.G. Park, p. 100, AGU, Washington, D.C., 1978.

Helliwell, R. A., S. B. Mende, J. H. Doolittle, W. C. Armstrong, and D. L. Carpenter, Correlations between λ4278 optical emissions and VLF wave events observed at $L \simeq 4$ in the Antarctic, *J. Geophys. Res., 85*, 3376, 1980.

Helliwell, R.A., U.S. Inan, J.P. Katsufrakis, and D.L. Carpenter, Beat excitation of whistler mode sidebands using the Siple VLF transmitter, *J. Geophys. Res., 91*, 143, 1986*a*.

Helliwell, R. A., D. L. Carpenter, U. S. Inan, and J. P. Katsufrakis, Generation of band limited VLF noise using the Siple transmitter: A model for magnetospheric hiss, *J. Geophys. Res., 91,* 4381, 1986*b*.

Imhof, W. L., J. B. Reagan, H. D. Voss, E. E. Gaines, D. W. Datlowe, J. Mobilia, R. A. Helliwell, U. S. Inan, J. P. Katsufrakis, and R. G. Joiner, Direct observation of radiation belt electrons precipitated by controlled injection of VLF signals from a ground-based transmitter, *Geophys. Res. Lett., 10*, 361, 1983.

Inan, U. S., and R. A. Helliwell, DE-1 observations of VLF transmitter signals and wave-particle interactions in the magnetosphere, *Geophys. Res. Lett., 9*, 917, 1982.

Inan, U. S., H. C. Chang, R. A. Helliwell, J. P. Katsufrakis, W. L. Imhof, J. B. Reagan, M. Walt, D. W. Datlowe, and J. Mobilia, Wave-induced precipitation as a loss process for radiation belt particles, *Adv. Space Res., 5*, 243, 1985.

Kimura, I., H. Matsumoto, T. Mukai, K. Hashimoto, T. F. Bell, U. S. Inan, R. A. Helliwell, and J. P. Katsufrakis, EXOS-B/Siple Station VLF wave-particle interaction experiments, 1, General description and wave-particle correlations, *J. Geophys. Res., 88*, 282, 1983.

Matthews, J. P., Y. Omura, and H. Matsumoto, A study of par-

ticle trapping by whistler mode waves in the geomagnetic field: The early development of the VLF quiet band, *J. Geophys. Res., 89*, 2275, 1984.

Matsumoto, H., K. Hashimoto, and I. Kimura, Dependence of coherent nonlinear whistler interaction on wave amplitude, *J. Geophys. Res., 85*, 644, 1980.

Park, C. G., Generation of whistler mode sidebands in the magnetosphere, *J. Geophys. Res., 86*, 2286, 1981.

Paschal, E.W., and R.A. Helliwell, Phase measurements of whistler mode signals from the Siple VLF transmitter, *J. Geophys. Res., 89*, 1667, 1984.

Raghuram, R., R.L. Smith, and T.F. Bell, VLF Antarctic antenna: Impedance and efficiency, *IEEE Trans. Antennas Propag., AP-22*, 334, 1974.

Raghuram, R., T. F. Bell, R. A. Helliwell, and J. P. Katsufrakis, Quiet band produced by VLF transmitter signals in the magnetosphere, *Geophys. Res. Lett., 4*, 199, 1977.

Rastani, K., U. S. Inan, and R. A. Helliwell, DE 1 observations of Siple transmitter signals and associated sidebands, *J. Geophys. Res., 90*, 4128, 1985.

Rosenberg, T. J., R. A. Helliwell, and J. P. Katsufrakis, Electron precipitation associated with discrete very low frequency emissions, *J. Geophys. Res., 76*, 8445, 1971.

Sa, L.A.D., and R. A. Helliwell, Structure of VLF whistler mode sideband waves in the magnetosphere, *J. Geophys. Res., 93*, 1987, 1988.

Sonwalkar, V. S., and U. S. Inan, Measurements of Siple transmitter signals on the DE 1 satellite: Wave normal direction and antenna effective length, *J. Geophys. Res., 91*, 154, 1986.

Sonwalkar, V. S., T. F. Bell, R. A. Helliwell, and U. S. Inan, Direct multiple path magnetospheric propagation: A fundamental property of nonducted VLF waves, *J. Geophys. Res., 89*, 2823, 1984.

Stassinopoulos, E. G., L. J. Lanzerotti, and T. J. Rosenberg, Temporal variations in the Siple Station conjugate area, *J. Geophys. Res., 89*, 5655, 1984.

R.A. Helliwell, STAR Laboratory, Stanford University, Stanford, CA 94305.

(Received January 11, 1988;
accepted April 5, 1988.)